Final Technical Report

ADVANCED DIAGNOSTICS FOR REACTING FLOWS

Grant AFOSR F49620-98-1-0010

Prepared for

AIR FORCE OFFICE OF SCIENTIFIC RESEARCH

For the Period

November 1, 1997 to November 30, 2000

Submitted by

R. K. Hanson, Principal Investigator

REPORT DOCUMENTATION PAGE

AFRL-SR-BL-TR-01-

0414

1. REPORT DATE (DD-MM-YYYY)	2. REPORT TYPE	3. DATES COVERED (From - To)
30-11-2000	Final Technical	1-11-1997 - 30-11-2000

4. TITLE AND SUBTITLE
(U) Advanced Diagnostics for Reacting Flows

5a. CONTRACT NUMBER

5b. GRANT NUMBER
F49620-98-1-0010

5c. PROGRAM ELEMENT NUMBER
61102F

6. AUTHOR(S)
Ronald K. Hanson

5d. PROJECT NUMBER
2308

5e. TASK NUMBER
BX

5f. WORK UNIT NUMBER

7. PERFORMING ORGANIZATION NAME(S) AND ADDRESS(ES)

Stanford University
Mechanical Engineering
Department
Stanford CA 94305-3032

8. PERFORMING ORGANIZATION REPORT NUMBER

9. SPONSORING / MONITORING AGENCY NAME(S) AND ADDRESS(ES)
AFOSR/NA
801 North Randolph Street
Room 732
Arlington VA 22203-1977

10. SPONSOR/MONITOR'S ACRONYM(S)

11. SPONSOR/MONITOR'S REPORT NUMBER(S)

12. DISTRIBUTION / AVAILABILITY STATEMENT

Approved for public release; distribution is unlimited

13. SUPPLEMENTARY NOTES

14. ABSTRACT

Advanced optical diagnostic techniques relevant to propulsion were investigated. The techniques studied were based on laser spectroscopy, with emphasis on spectrally-resolved absorption and laser-induced fluorescence (LIF). Laser sources included tunable cw near-infrared diode lasers and tunable (or fixed-wavelength) pulsed lasers operated at ultraviolet and infrared (IR) wavelengths. The cw lasers were spectrally narrow, allowing study of innovative diagnostics based on spectral line shapes, while the pulsed lasers provided intense bursts of photons needed for techniques based on LIF. Accomplishments of note included: development of new diagnostic methods based on the first demonstration of IR planar laser-induced fluorescence (IR-PLIF); demonstration of ultra-sensitive detection of CO through the first use of 2.3-micron diode lasers for combustion applications; initial measurements of absorption and fluorescence properties of 3-pentanone, enabling evaluation of this species as a flow tracer in air-breathing propulsion flowfields; continued development of novel facilities for studies of combustion gas spectroscopy at high pressures; and final development and testing of a new sensor for monitoring velocity in hypervelocity streams via Doppler-shifted absorption of 770 nm diode laser light.

15. SUBJECT TERMS
Optical diagnostics, diode lasers, planar laser-induced fluorescence, hypervelocity flows, absorption

16. SECURITY CLASSIFICATION OF:			17. LIMITATION OF ABSTRACT	18. NUMBER OF PAGES	19a. NAME OF RESPONSIBLE PERSON
a. REPORT	b. ABSTRACT	c. THIS PAGE			Julian M. Tishkoff
Unclassified	Unclassified	Unclassified	UL	51	19b. TELEPHONE NUMBER (include area code) (703) 696-8478

Table of Contents

1.0 Introduction

Advanced optical diagnostic techniques relevant to propulsion were investigated. The techniques studied were based on laser spectroscopy, with emphasis on spectrally-resolved absorption and laser-induced fluorescence (LIF). Laser sources included tunable cw near-infrared diode lasers and tunable (or fixed-wavelength) pulsed lasers operated at ultraviolet and infrared (IR) wavelengths. The cw lasers were spectrally narrow, allowing study of innovative diagnostics based on spectral line shapes, while the pulsed lasers provided intense bursts of photons needed for techniques based on LIF. Accomplishments of note included: development of new diagnostic methods based on the first demonstration of IR planar laser-induced fluorescence (IR-PLIF); demonstration of ultra-sensitive detection of CO through the first use of 2.3-micron diode lasers for combustion applications; initial measurements of absorption and fluorescence properties of 3-pentanone, enabling evaluation of this species as a flow tracer in air-breathing propulsion flowfields; continued development of novel facilities for studies of combustion gas spectroscopy at high pressures; and final development and testing of a new sensor for monitoring velocity in hypervelocity streams via Doppler-shifted absorption of 770 nm diode laser light.

2.0 Project Summaries

2.1 Imaging of CO and CO_2 Using Infrared PLIF

Background

Many critical combustion species, including important combustion products and fuels (CO, CO_2, H_2O, and CH_4), do not have accessible single-photon electronic spectra that would permit relatively facile planar laser-induced fluorescence (PLIF) imaging. Though PLIF diagnostics have played a key role in design and analysis of combustion systems, providing spatially and temporally resolved field information, they have not in the past been able to provide images of these critical species. However, new state-of-the-art laser sources produce the infrared light intensity needed for PLIF, and infrared camera systems with suitable integration properties are becoming available at a variety of wavelengths. Exploiting these new technological developments with novel excitation and detection strategies to avoid infrared flame emission, we have made significant progress in development of infrared PLIF.

During the current funding period we have demonstrated the first infrared (IR) PLIF diagnostics schemes suitable for imaging the class of species (including CO, CO_2, H_2O, and CH_4) which lack convenient UV transitions. These strategies take advantage of recent advances both in IR laser sources (based on optical parametric oscillators) and IR

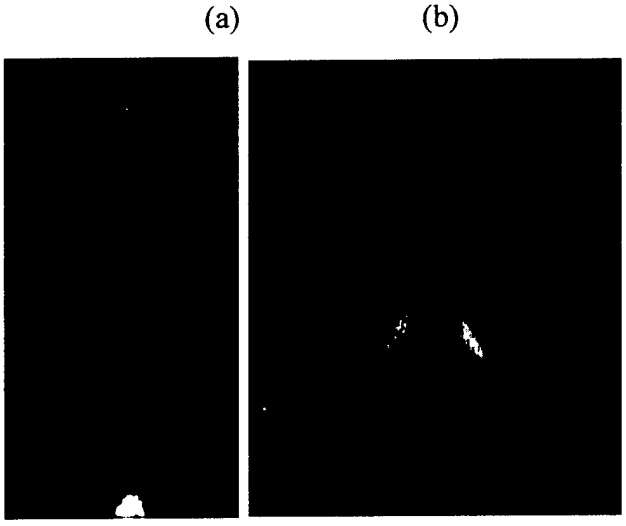

Fig. 2.1.1. (a) At left: single-shot visualization of the fuel region of a CO/Ar/H_2 laminar diffusion flame generated using IR PLIF of CO. (b) At right: single-shot visualization of mixing of a forced CO_2/Ar jet in air generated using IR PLIF of CO_2.

cameras (based on indium antimonide focal plane arrays). Our initial demonstrations of IR PLIF highlight the accomplishments during the current grant. We expect that, upon development, these IR PLIF diagnostics will eventually be possible for a variety of purposes, e.g., to identify toxic formation/removal zones (CO), localize regions of heat

release and fuel oxidation (CO_2, H_2O), and evaluate fuel mixing processes (CO, CH_4), all of which expand the Air Force's ability to design and analyze air-breathing propulsion systems.

Competing diagnostics for imaging of species that lack convenient UV transitions include spontaneous Raman scattering [1], and multi-photon (nonlinear) PLIF techniques [2]. Raman is linear and easily modeled but generates weak signals and can be limited in implementation by a variety of spectral interferences; multi-photon LIF, despite its usefulness for point measurements [2] and imaging [3] of CO in flames, suffers (for most species, *e.g.*, H_2O [4]) from strong nonlinearity and low signal due to the predissociative nature of the excited state. In contrast to Raman and multi-photon techniques, IR PLIF is a *linear* technique that offers high signal levels (several orders more signal photons than Raman) and is applicable to all IR-active species including CH_4, CO_2, and H_2O. High signal levels imply high SNR and dynamic range, while linearity permits easy interpretation of data and increased quantitative accuracy. Figure 2.1.1 shows two sample experimental realizations (discussed in detail later in this section) of single-shot IR PLIF imaging of CO and CO_2 in flame and room temperature conditions respectively. The quality of these images indicates the potential for IR PLIF to provide spatially and temporally resolved imaging of CO and CO_2 in flows pertinent to combustion. Work under the current contract has reported initial imaging efforts for CO [5]; and, more recently, has presented new results with both single- and dual-camera techniques for imaging of CO and CO_2 in steady and unsteady flows of interest to the combustion community [6-8].

Theory

Our initial modeling and experimentation focused on CO due to its well-understood spectroscopy, simple vibrational structure and energy transfer mechanisms, and conveniently accessed absorption spectra. We quantify fluorescence signal through the use of the fluorescence equation:

$$S_f = \frac{E}{h\upsilon} \; gSl \; \frac{P\chi_{\text{abs}}}{kT} \; \phi\eta_c \,, \qquad \text{(Eqn. 2.1.1)}$$

where S_f (photons per camera pixel) is the fluorescence signal; E (J) is the laser pulse energy incident on the imaged pixel volume; $h\nu$ (J) is the energy per photon; g (cm) is the convolution of the laser and absorption lineshapes; S (cm) is the line strength per number density, which takes into account the Boltzmann fraction of the absorbing species in the lower state of the laser transition; l (cm) is the length of the area imaged onto the pixel; $P\chi_{abs}/kT$ (cm^{-3}) is the number density of the species; ϕ is the fluorescence quantum yield; and η_c is the collection efficiency of the optics and camera. The fluorescence signal for isobaric flows is a function of imaged species mole fraction, bath gases (through energy transfer rates and their effect on fluorescence yield), and temperature (through energy transfer rates, number density, and state distributions). For species imaging, short exposure times can be used to minimize sensitivity to collisional environment, while judicious choice of excitation line can be used to control temperature dependence. The strengths of vibrational molecular transitions (which determine the line strength S and are

a component of the fluorescence yield ϕ) are weak as compared to electronic transitions; however, this weakness is offset in certain situations by the large mole fractions present for the species of interest (*e.g.*, CO, CO_2) in typical flows, as well as the slow nature of typical de-excitation processes which limit the fluorescence yield ϕ.

The parameters in Eqn 2.1.1 are easily quantified with the possible exception of the fluorescence yield ϕ, which may be written as an integration of the relevant excited state populations and spontaneous emission coefficients over the camera integration time:

$$\phi = \sum_j \int_o^\tau A_j \frac{n_j}{N} dt . \qquad \text{(Eqn. 2.1.2)}$$

Here fluorescence is summed over j excited states. A_j is the summed Einstein A coefficient for all emitting transitions from the state j consistent with the spectral collection bandwidth, n_j/N is the instantaneous population in the excited state normalized by the total number of absorbed laser photons, and τ is the camera integration time.

Differences in scale between the camera integration time and the emissive state radiative and collisional lifetimes lead to simpler expressions that describe the limiting behavior of Eqn. 2.1.2. For traditional PLIF techniques, which employ electronic transitions, the excited state population undergoes simple exponential decay dictated by the collisional quench rate Q, since the collisional quenching is typically fast (~1 ns) when compared to either the radiative lifetime (~1 μs) or the camera gate time (20-300 ns). In this case, we recover the familiar equation for fluorescence yield:

$$\phi = \frac{A}{Q} . \qquad \text{(Eqn. 2.1.3)}$$

Equation 2.1.3, though, typically does *not* properly describe the fluorescence yield for IR PLIF techniques, because the vibration-to-translation (V-T) energy transfer which serves to remove vibrational energy from the system is often slow (~1–100 μs) as compared to the camera integration time (~0.1–10 μs). Vibration-to-vibration (V-V) energy transfer is often fast, but it serves only to rearrange the vibrational energy and does not provide strong coupling to the translational and rotational modes. Thus, as the camera integration time is shortened below the V-T decay time, the limit is approached in which the excited state population stays constant during the camera integration time. In this case Eqn. 2.1.2 approaches

$$\phi = A\tau . \qquad \text{(Eqn. 2.1.4)}$$

This limit is advantageous, because fluorescence quantum yield becomes independent of excited state de-excitation rates and is therefore independent of both bath gas and temperature.

We turn now to a more detailed examination of the general energy transfer processes described above. Following laser excitation, typically the pumped vibrational mode equilibrates itself first, followed by intermolecular V-V equilibration with near-resonant modes of similar energy (*e.g.*, CO, N_2, ν_3 of CO_2), followed by relatively slower V-V/T equilibration with nonresonant vibrational modes and the translational/rotational modes. Collisional depletion of the pumped mode (and coupled modes emitting within the collection bandwidth) competes with spontaneous emission to determine the fluorescence quantum yield. A schematic diagram of these energy transfer processes is shown in Fig 2.1.2.

Characteristic times for vibrational energy transfer (VET) from CO to common species for 1 atm and typical concentrations are shown in Fig. 2.1.3. Since CO has only one vibrational frequency and rather large energy spacing, species without near-resonant modes (*e.g.*, inert gases, O_2) play little role in extracting energy from CO at these temperatures and are therefore not shown. Temperature dependences are minor, as expected, due to the dominance of near-resonant V-V transfer mechanisms which stem in large part from long-range interactions rather than energetic collisions.

A model of the vibrational energy transfer has been developed so as to quantify ϕ as a function of bath gas, temperature, pressure, and camera integration time. This model uses a rate equation formulation (CHEMKIN) to solve for the vibrational-state-specific populations as a function of time, including effects of both V-V and V-T processes. For simplicity, the model assumes translational and rotational equilibrium.

To enable implementation using the CHEMKIN interface and solver, functions are fit to experimental or computational reaction rate data from a variety of references. When necessary (rarely), literature results are extrapolated using SSH theory. The thermodynamic database input to CHEMKIN is modified slightly to treat the molecules on a vibrational-state-specific basis.

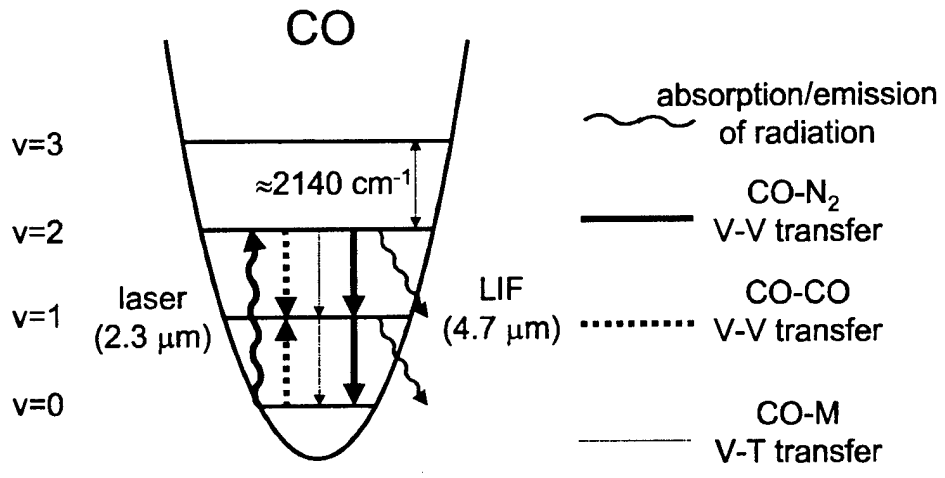

Fig. 2.1.2. Energy transfer diagram for CO molecules during CO LIF.

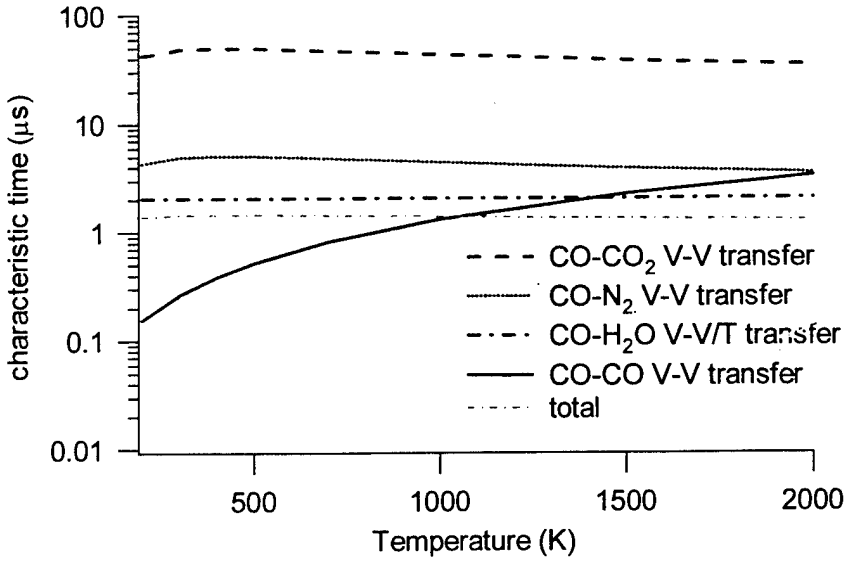

Fig. 2.1.3. Calculated characteristic times (1/transfer rate) of VET from CO to common species as a function of temperature at 1 atm. A mixture of 5% CO, 10% CO_2, 10% H_2O, 75% N_2 is assumed. Components that remove energy from CO are shown with dotted/dashed lines and the summed transfer is shown in grey. The solid red line indicates CO-CO V-V transfer which tends to equilibrate the CO vibrational mode but does not serve as a quenching mechanism.

A simple example of fluorescence quantum yield calculations is shown in Fig. 2.1.4 for CO using a 1 μs exposure time. This example highlights the advantages of using exposure times that are shorter than excited state lifetime. In addition to being desirable for time resolution and reduction of background luminosity, short exposures cause ϕ to approach the limit of Eqn. 2.1.3 and thus lead to a fluorescence quantum yield that is only a weak function of composition and temperature. In particular, changes in H_2O mole fraction that otherwise might generate one or two orders of magnitude change in signal levels generate only ±15% variations when carefully chosen exposure times are used. In complicated flowfields, where detailed calculations of fluorescence yield are difficult or impossible, quantitative *a priori* calculations of ϕ may be made feasible through use of short exposure times.

Using excitation of the first overtone near 2.3 μm and collection of the fundamental near 4.7 μm (Fig. 2.1.2), we have demonstrated IR PLIF imaging of CO in flows ranging from room-temperature mixing to laminar diffusion flames (Fig. 2.1.1a). Challenges include (a) generation of adequate signal level, (b) discrimination of PLIF signal from background luminosity, and (c) interpretation of signal levels in terms of meaningful flow properties. Signal level has been achieved primarily through the use of the aforementioned high-pulse-energy infrared optical parametric amplifiers. Signal discrimination has been achieved through use of state-of-the-art IR camera technology which allows for short exposure times, along with use of dual-camera configurations for common-mode rejection of ambient luminosity. Signal interpretation has been achieved through detailed modeling of energy transfer during absorption and fluorescence processes.

Based on our successes in CO imaging, we have turned to imaging of CO_2 (Fig. 2.1.1b) which, due to its polyatomic nature, has more complicated vibrational structure and energy transfer mechanisms. In the case of CO_2, energy transfer occurs both via near-resonant transfer (upon collisions with CO and N_2) and via non-resonant intermodal V-V transfer (upon collisions with any molecule M), both of which serve to deplete states with asymmetric stretch (ν_3). Because of the efficiency of intermodal V-V transfer (defined here as transfer of energy between modes, *e.g.*, the transfer caused by a collisional $CO_2(00^01)\rightarrow CO_2(11^10)_I$ transition), the energy gaps associated with the vibrational transfer mechanisms are smaller, and energy resonance plays a less important role in dictating the relative speed of different vibrational energy transfer mechanisms. Because energy resonances are less important, rates of energy transfer are less dependent on the species makeup of the bath gas.

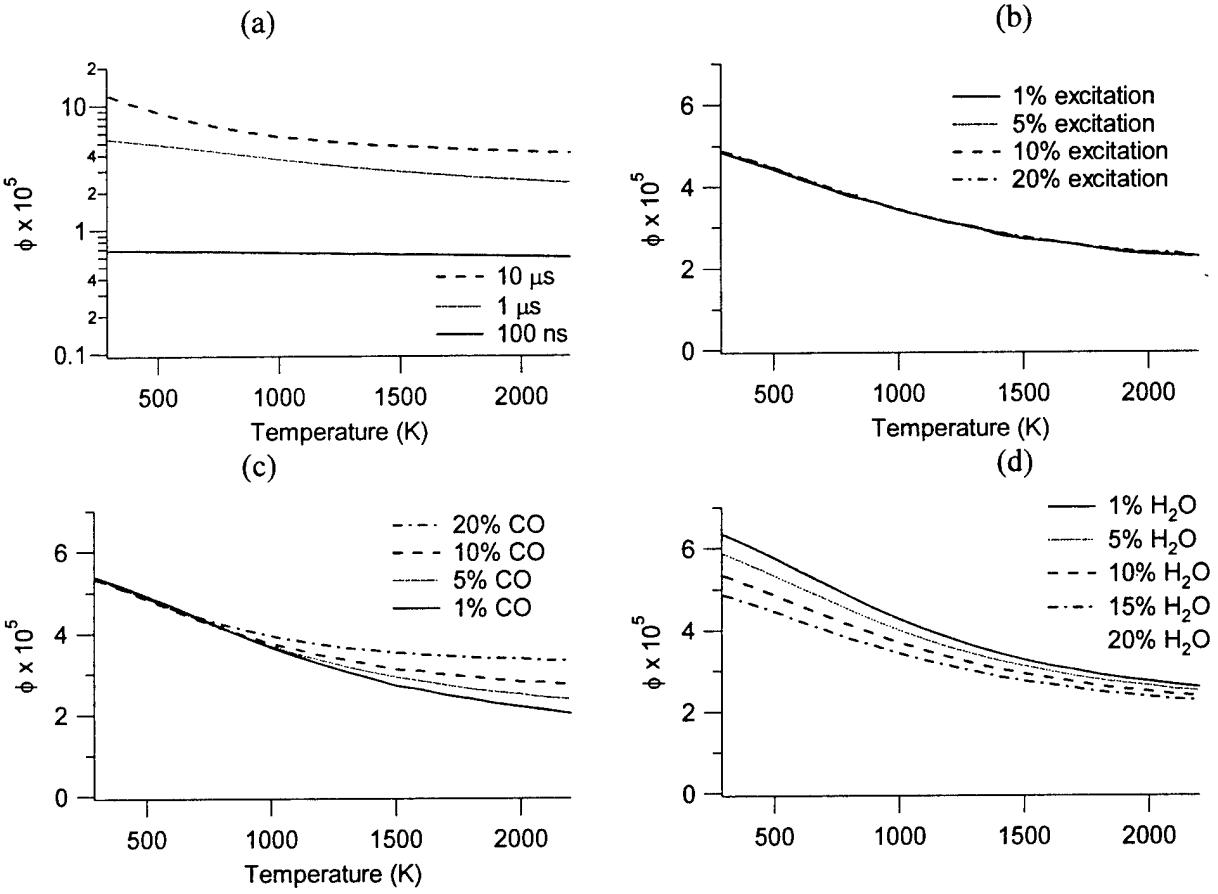

Fig. 2.1.4. CO fluorescence quantum yield as a function of temperature and composition. Nominal parameters: 1 μs exposure, 10% excitation, mixture of 5% CO, 15% CO_2, 15% H_2O in N_2. Each graph shows ϕ as one parameter is changed and others held constant. (a): effect of exposure time, (b): effect of strength of excitation, (c): effect of CO mole fraction, (d): effect of H_2O mole fraction.

Characteristic times for VET from CO_2 to common species at typical concentrations are shown in Fig. 2.1.5. The primary energy transfer processes are resonant transfer with N_2 and collisional intermodal V-V transfer. Temperature

dependences are stronger for CO_2 due to the nonresonant nature of the intermodal V-V transfer which is therefore more dependent on collision energy.

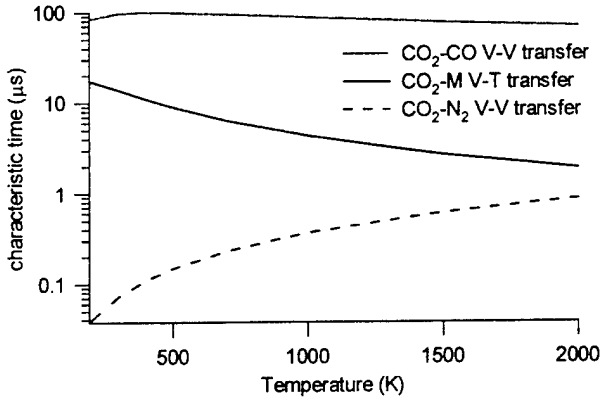

Fig. 2.1.5. Calculated characteristic times (1/transfer rate) of VET from CO_2 to common species as a function of temperature at 1 atm. Mixture of 5% CO, 10% CO_2, 10% H_2O, 75% N_2.

During the course of our investigation of CO imaging techniques, we realized that the vibrational "quenching" processes provide an opportunity for new diagnostic strategies, as the vibrational energy added to CO via laser excitation can be transferred to other molecules which then fluoresce. Of specific note is our observation that after excitation of CO one can separately collect both CO *and* CO_2 fluorescence; the former signal approximates the CO concentration and the latter the local CO/CO_2 concentration product. This new diagnostic strategy has been exploited to image both the fuel region (CO) and fuel-product interface region (CO_2) of a $CO/Ar/H_2$ laminar diffusion flame. Results are shown in the following sections.

Imaging Setup and Techniques

A typical setup for IR PLIF experimentation is shown in Fig. 2.1.6, illustrating the use of our recent equipment advances. The optical parametric oscillator/amplifier (OPO/OPA) system is based upon a commercial product and modified to extend the wavelength range as well as increase power. This IR laser source is a 10 Hz, nanosecond-pulse system whose wavelength is controlled by a 532 nm-pumped, grating-tuned optical parametric oscillator (Continuum Mirage 3000) and whose power is generated and amplified by four 1064 nm-pumped optical parametric amplifier stages. This system generates high pulse energies (10-20 mJ) in the 1.3-4.7 μm region. The oscillator signal beam (720-740 nm) from the laser is monitored using a commercial interferometer (Burleigh WA-4500) to ensure single-longitudinal-mode operation (400 MHz linewidth) and to determine the wavelength of the mid-IR beam. The laser is grating-tuned to absorption lines of overtone or combination bands of CO or CO_2 in the 2.0–2.4 μm region and centered on a specific line by maximizing LIF from a reference cell. The mid-IR beam is then expanded vertically and focused horizontally using calcium fluoride cylindrical lenses to generate a 4 cm high laser sheet with a 450 μm (FWHM) waist, 50 mm Rayleigh range, and nominal pulse energy of 12 mJ. PLIF signal is collected through bandpass filters and f/2.5 singlet CaF_2 lenses onto one or two 256x256 InSb cameras with submicrosecond gating capabilities (Santa Barbara

Focalplane SBF 134). The IR camera systems are sensitive from 700 nm-5.5μm and have a specified minimum gate time near 300 ns. This short minimum gate time enables rejection of unwanted light sources. The InSb cameras have been designed specifically to provide short exposure times, and are therefore capable of submicrosecond exposures without bias changes or other nonlinear effects common to many IR cameras.

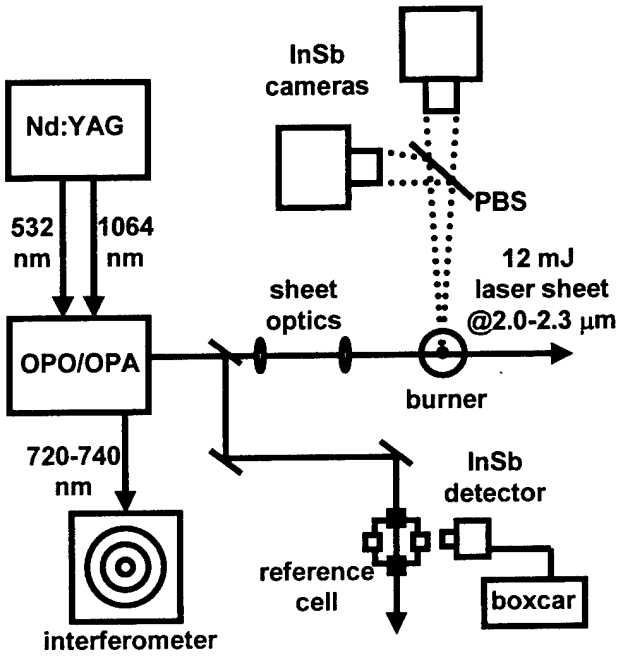

Fig. 2.1.6. Experimental setup for imaging experiments. PBS-pellicle beamsplitter. InSb cameras (Santa Barbara FocalPlane SBF134) have following characteristics: 0.7–5.3 μm sensitivity range; 30 μm pixels; 85 % quantum efficiency; 130 ns minimum integration time setting; 300 Hz maximum frame rate.

Typical imaged region sizes are roughly 2.5x2.5 cm, and typical integration times range from 1 to 20 μs. Standard techniques as described in many other sources (*e.g.*, [5,9,10]) are used to correct each image individually for laser attenuation, laser sheet inhomogeneity, and background signals of both optical and electrical nature. A strictly linear analysis is used (Eqn. 2.1.1) which assumes negligible perturbation of the molecular state distribution. The validity of this approximation was verified by (a) detailed rate equation analysis using rotational energy transfer rates inferred from pressure-broadened linewidths and line mixing and (b) measurements of LIF linearity.

For each camera and filtering scheme, pixel-by-pixel responsivity and gain are calibrated by taking images of uniform temperature solid (Lambertian) graybody emitters. Errors caused by approximating these as isotropic sources were negligible for the collection optics used in this work but could be important if extremely fast optics are used.

Imaging Experiments

Two flow conditions are highlighted in this report: (a) a 6 mm diameter, room-temperature, forced jet, in which a valve is quickly opened and closed, superimposing an impulse onto a laminar jet flow, thus forming one or more vortex rings; and (b) a laminar flame with 50%CO/50%Ar as fuel (trace H_2 added) with an air coflow. This flame could be perturbed to explore unsteady effects as desired, although only steady results are presented here.

Three excitation/collection schemes are employed: (a) excitation of CO via the ground state 2ν band near 4300 cm^{-1} (2.35 μm) and collection of CO fluorescence from fundamental transitions near 4.7 μm; (b) excitation of CO_2 via the $(20^01)_{II}\leftarrow(00^00)$ band near 5000 cm^{-1} (2.0 μm) and collection of CO_2 ν_3 fluorescence near 4.3 μm; (c)

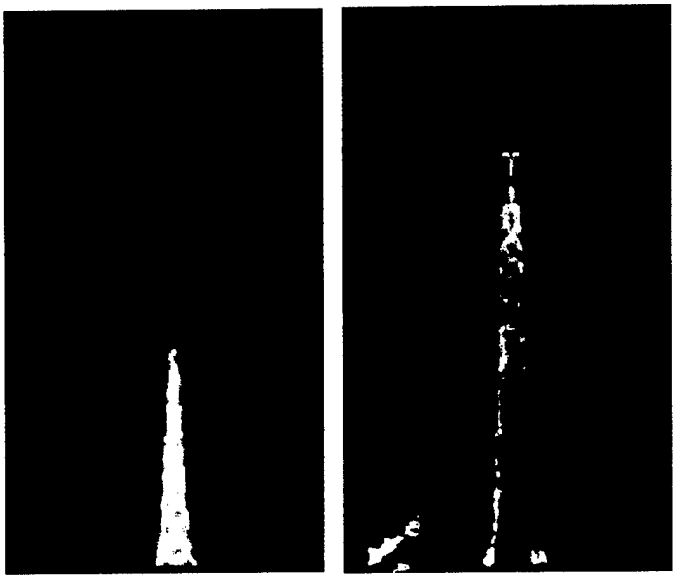

Figure 2.1.7. At left, a: CO fluorescence (single shot) from fuel region of a CO/Ar/H_2 laminar diffusion flame after excitation of CO. At right, b: CO_2 fluorescence (20-frame average) indicating fuel-product interface from the same flow using *identical laser excitation of CO.*

excitation of the 2ν band of CO followed by rapid CO-CO_2 V-V transfer and collection of CO_2 fluorescence near 4.3 μm. Scheme (a) (Fig. 2.1.1a) indicates presence of CO, scheme (b) (Fig. 2.1.7b) indicates the presence of CO_2, and scheme (c) (Fig. 2.1.1b) indicates the presence of both CO *and* CO_2. Through the use of two cameras, the combination of schemes (a) and (c) allows for simultaneous imaging of both CO and CO_2 with single laser excitation.

Representative peak SNR ratios for room-temperature images (Fig. 2.1.1b) range from 150–200. Signal levels of the images presented here can be used to infer a detection limit (SNR=1) for the present experimental setup of 1350 ppm (CO) and 950 ppm (CO_2) at 300 K. Presentation in these figures is qualitative (color table corresponds to PLIF signal), although it should be noted that techniques and results for quantitative presentation have been presented previously [5].

A laminar coflowing $CO/Ar/H_2$ flame was used to demonstrate imaging of CO (fuel) and CO_2 (products) in a flame condition. Excitation schemes (a) and (c) were employed. Because the flame generates hot CO and CO_2 which emit within the collection bandwidth, common-mode rejection of flame luminosity was achieved by subtracting an image taken without laser excitation from the PLIF image. Fig. 2.1.7 shows typical CO and CO_2 imaging results. In these images, CO represents fuel and CO_2 represents the fuel-product interface. The fuel region is clearly identified by the CO PLIF signal (which scales with CO concentration), while fuel and product regions are demarcated by the CO_2 signal (which scales with the product of CO and CO_2 concentrations).

Section 2.1 References

1. Long, M., Fourguette, D. and Escoda, M., "Instantaneous Ramanography of a Turbulent Diffusion Flame," *Optics Lett.* **8**, 244-246 (1983).

2. Barlow, R., Frank, J. and Fiechtner, G., "Comparison of CO Measurements by Raman Scattering and Two-Photon LIF in Laminar and Turbulent Methane Flames," Spring Meeting, WSSCI, Paper No. WSS/CI 98S-19, (1998).

3. Haumann, J., Seitzman, J. M. and Hanson, R. K., "2-Photon Digital Imaging of CO in Combustion Flows Using Planar Laser-Induced Fluorescence," *Optics Lett.* **11**, 776-778 (1986).

4. Juhlin, G., Neij, H., Versluis, M., Johansson, B., and Alden, M., "Planar Laser-Induced Fluorescence of OH to Study the Influence of Residual Gases on Cycle-to-Cycle Variations in SI Engines," *Comb. Sci. Tech.* **132**, 75-97 (1998).

5. Kirby, B. and Hanson, R. K., "Planar Laser-Induced Fluorescence Imaging of Carbon Monoxide Using Vibrational (Infrared) Transitions," *Appl. Phys. B* **69**, 505-507 (1999).

6. Kirby, B. and Hanson, R. K., "Design and Analysis of Excitation Schemes for IR PLIF Imaging of CO and CO_2," submitted to *Appl. Optics*, September 2000.

7. Kirby, B. and Hanson, R. K., "CO_2 Imaging Using Saturated Planar Laser-Induced Vibrational Fluorescence," submitted to *Appl. Optics*, September 2000.

8. Kirby, B. and Hanson, R. K., "Imaging of CO and CO_2 Using Infrared Planar Laser-Induced Fluorescence," *28th Proc. Comb. Inst.*, in press.

9. Seitzman. J. and Hanson, R. K., "Planar Fluorescence Imaging in Gases," *Experimental Methods for Flows with Combustion.* Academic Press, London, 1993.

10. McMillin, B. K., Palmer, J. L. and Hanson, R. K., "Temporally Resolved, 2-Line Fluorescence Imaging of NO Temperature in a Transverse Jet in a Supersonic Cross-Flow," *Appl. Optics* **32**, 7532-7545 (1993).

2.2 Ketone Photophysics for Quantitative PLIF Diagnostics

This section reports work conducted to characterize 3-pentanone photophysics, with the objective of establishing improved temperature and mixture fraction PLIF imaging in propulsion-related flows. Successful results from our AFOSR-sponsored research on acetone, including demonstrations and modeling, have lent insight and laid the groundwork for similar experimentation, modeling, and imaging demonstrations of 3-pentanone.

Acetone (CH_3COCH_3) has long been popular as a PLIF tracer because it is a readily available, relatively safe chemical that yields strong non-resonant fluorescence signals when pumped with high-power UV lasers. Furthermore, intersystem crossing from the excited singlet to the triplet state limits signal dependence on the collisional environment. The fundamental photophysical studies at Stanford examining the effect of temperature and pressure on fluorescence signal have led to new single and dual-wavelength acetone PLIF techniques which provide useful measurements of temperature and mole fraction in a variety of flows. This work is detailed in references 1-5. Fig. 2.2.1 provides example results of a heated turbulent jet. The incident 65 mJ laser sheets at 248 and 308 nm were separated by 800 ns (a time small relative to the time scale of the flow). Fluorescence from each wavelength was then collected in separate frames by a fast interline transfer CCD camera. Through techniques described below, the fluorescence signal from these two images is then mapped to temperature and concentration. Resolution limits are about 2% for the jet fluid fraction and 7 K for the temperature image—figures demonstrating excellent potential for this technique in flows of practical interest, e.g. the mixing regions of combustors.

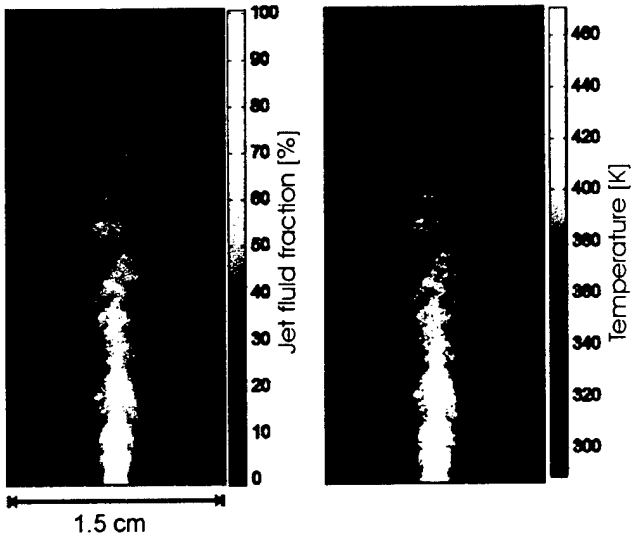

Fig. 2.2.1. T and χ images for an atmospheric acetone-seeded, heated, turbulent jet. Resolution is about 2% in jet fluid fraction and about 7 K in temperature.

In addition to the development of new diagnostic techniques, the photophysical data gathered from acetone experiments have been applied to the development of a fluorescence model accounting for wavelength, temperature, pressure, and bath gas effects on fluorescence [1-2]. Such a model provides not only physical understanding of the processes involved but also predictive capability beyond available experimental data. Furthermore, we believe that other ketones like 3-pentanone ($C_2H_5COC_2H_5$) are likely to follow a similar pattern of behavior.

3-pentanone, because it is slightly larger and heavier than acetone, is better suited to tracking the heavier hydrocarbons so often found in combustion applications. The temperature and pressure dependences of its fluorescence signal have also been studied in a limited range (up to about 600K and 30 atm) with the goal of imaging the mixing processes in optically accessible cylinders [6-11]. Our present work seeks to extend the temperature range of photophysical studies to 900 K. We are continuing to gather data that will be applied to a general ketone fluorescence model, and simultaneously, we are working toward quantitative 3-pentanone PLIF in high-pressure, nonuniformly seeded, nonuniform temperature environment. This progress report describes the photophysical results and demonstration of quantitative 3-pentanone imaging that have recently occurred at Stanford during the latter part of this contract period.

Fluorescence Background

Fluorescence signal (in energy per unit volume) in the limit of weak excitation can be calculated from the following form of the fluorescence equation:

$$S_f = \eta_{opt} \frac{E}{hc/\lambda} n_{abs}(P,T)\,\sigma(\lambda,T)\,\phi(\lambda,P,T) \qquad \text{(Eqn. 2.2.1)}$$

Here, η_{opt} is the efficiency of the collection optics, E is the laser fluence [J/cm^2], and hc/λ is the energy [J] of a photon at the excitation wavelength λ. Quantities that vary with temperature, pressure, and composition are n_{abs}, the number density of absorbing molecules [cm^{-3}]; σ the molecular absorption cross-section of the tracer [cm^2]; and ϕ the fluorescence quantum yield. The number density n_{abs} is proportional to $\chi P / T$, where χ is the absorber mole fraction. The key to understanding fluorescence signal in terms of temperature and pressure lies in the behavior of the photophysical properties, σ and ϕ. From a diagnostic perspective, only the product of these properties needs to be known in order to map fluorescence signal to temperature information. For modeling and physical insight, each of these parameters should be isolated through measurements of absorption cross-sections and relative fluorescence signals.

Absorption Cross-section

Figure 2.2.2 shows the measured absorption cross-sections for 3-pentanone as a function of temperature when excited with 248 and 308 nm light. Previous data near room temperature from Martinez et al. [12] agree with these preliminary measurements. For 308 nm excitation, one sees an increase in absorption with temperature due in part to the increasing populations in the upper vibrational levels of the ground electronic state – a red shift that has been previously observed [7]. This explanation may not hold as well

for the increasing absorption at 248 nm because it is close to the blue tail of the absorption feature. An alternate explanation is the excitation of another electronic transition, one that may exist in the deep UV at low temperatures but like the studied feature, shifts to the red as temperature is increased. Further exploration of this phenomena and its effect on fluorescence may present new interpretations of the fluorescence signal from short wavelengths as well as opportunities for new diagnostics.

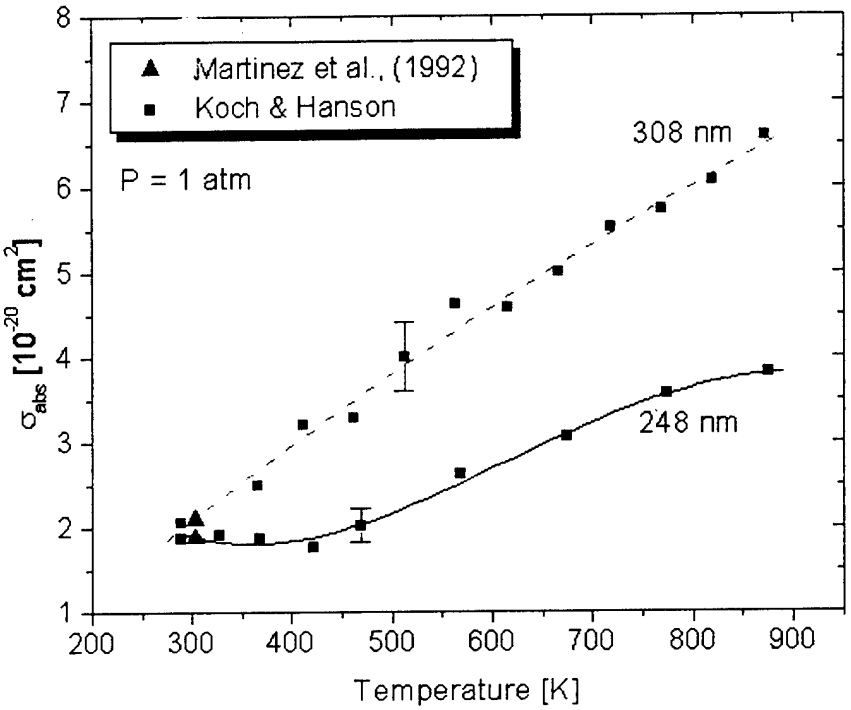

Fig. 2.2.2. 3-pentanone absorption cross-section per molecule for 248 and 308 nm excitation.

Fluorescence Signal

Figures 2.2.3 and 2.2.4 show the temperature dependence of 3-pentanone fluorescence (per unit mole fraction) between 300 and 875 K using excitation at 248 and 308 nm. Acetone data is shown on the same graphs for comparison. Though not shown here for the sake of brevity, data below 600 K agrees well with the previous work of others [6,7,10]. Excited with 248 nm, both ketones exhibit similar behavior, 3-pentanone being slightly more temperature sensitive below 600 K. A marked difference occurs when these ketones are excited with the longer wavelength as shown in Fig. 2.2.4. Of particular note is the relative temperature insensitivity of 3-pentanone fluorescence below 500 K. Such behavior indicates the potential for straightforward, single-line imaging of concentration in the presence of mild, low-temperature variations.

In situations where temperature information is desired and concentration is not uniform, ratioing the relative fluorescence signals of two different wavelengths results in a unique temperature dependence, independent of local concentration. The temperature mapping for 3-pentanone using a 308/248 nm fluorescence signal ratio is shown in Fig. 2.2.5. Again, acetone signal ratios using similar wavelengths are shown for comparison. Below 700 K 3-pentanone's temperature sensitivity is superior to acetone. However, above 700

K, these preliminary results indicate complex behavior for 3-pentanone. Reasons for this are currently unclear. There is reasonably large numerical uncertainty due to the low 248 nm signal; however, the rapid drop-off in the 308 nm signal as shown in Fig. 2.2.4 is indicative of more complex behavior than what has been observed in acetone.

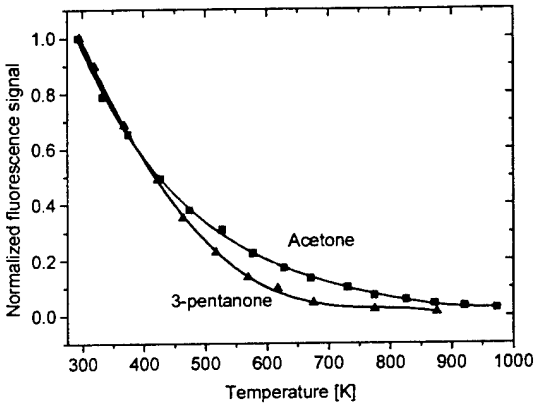

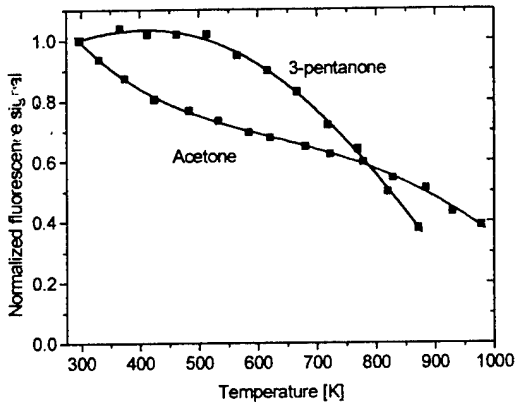

Left: Fig. 2.2.3. Relative ketone fluorescence signal per unit mole fraction excited with 248 nm light as a function of temperature. P = 1 atm. **Right: Fig. 2.2.4.** Relative ketone fluorescence signal per unit mole fraction excited with 308 nm light. P = 1 atm.

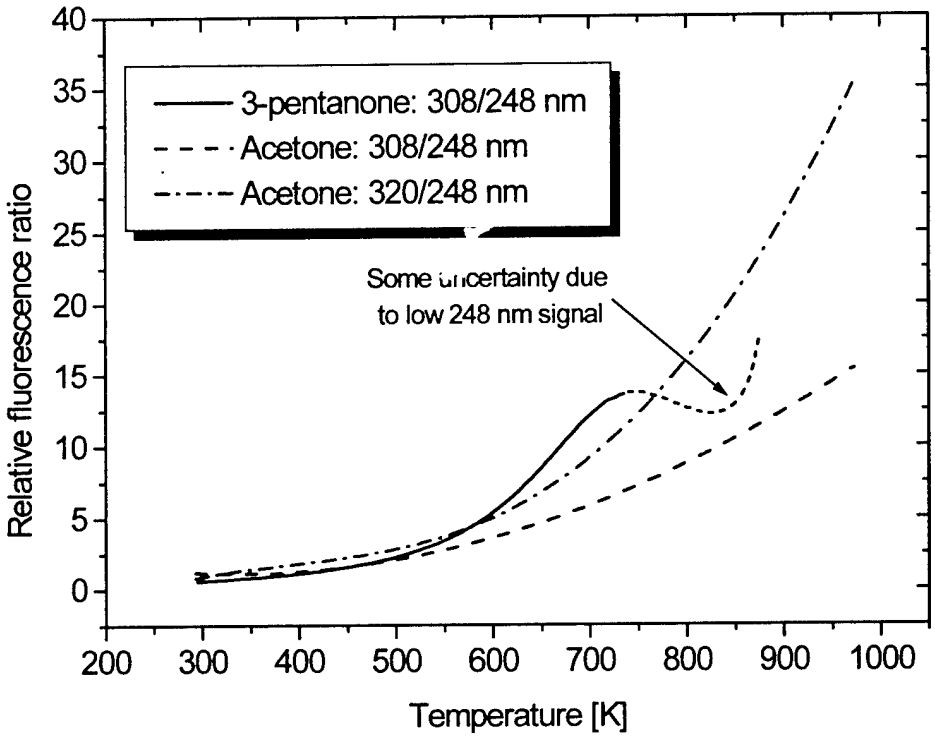

Fig. 2.2.5. Fluorescence signal ratio of ketones. Dashed portion of 3-pentanone line is uncertain due to low fluorescence signals from 248 nm excitation. P=1atm.

Single-Line Temperature Demonstration

As a first step toward 2-line imaging with 3-pentanone, a simple demonstration was performed on a heated jet similar to the acetone example above. Single wavelength PLIF of 3-pentanone provides temperature information in fields of uniform pressure and mole fraction. From Figs. 2.2.3 and 2.2.4, it is clear that 248 nm excitation provides the best sensitivity from 300 to about 600 K. In order to test the limits of this technique, the peak temperatures of the experiment were nominally set at 700 K.

As shown in Fig. 2.2.6, a heated nitrogen/3-pentanone jet with an unheated coflow provided a uniformly seeded flowfield. Excited with a 100 mJ laser sheet at 248 nm (~0.5 mm thick, 3.5 cm high), the fluorescence was captured by a Princeton Instruments MicroMAX 1300 YHS unintensified CCD camera with a gate time of 1 μs.

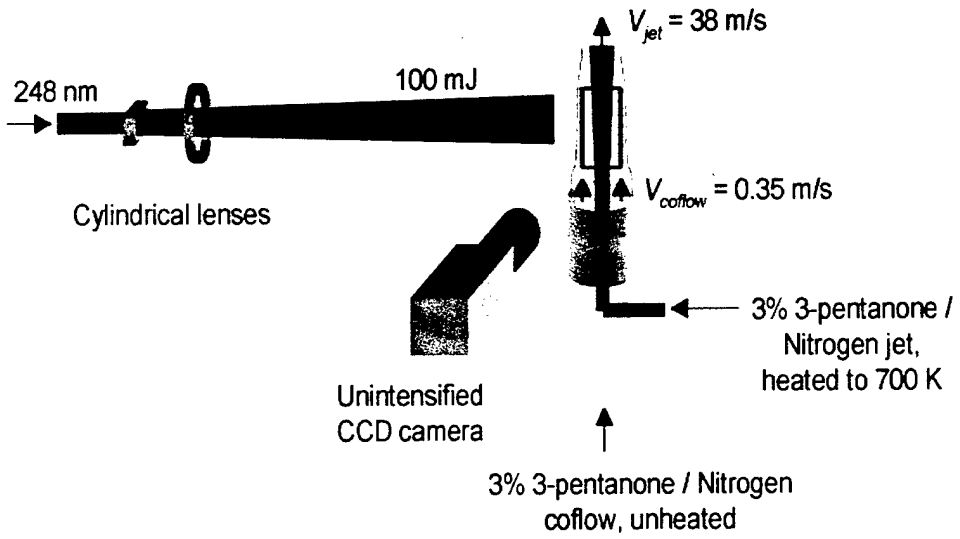

Fig. 2.2.6. Configuration for single-line temperature imaging of a uniformly seeded jet in coflow.

The image was then processed on a per-pixel basis by subtracting an average background signal, correcting for the laser sheet profile and variations in optical collection efficiency, and by calibrating the temperature-signal curve in Fig. 2.2.3 to a known location in the flow. Figure 2.2.7 is the result. In support of absolute accuracy, thermocouple measurements taken at the jet core match the average value of the image in the region to within 10 K. At 300 K, the temperature resolution was +/- 5 K, obtained by sampling small groups of pixels in the jet coflow. However, in the jet core, pixel-to-pixel variations jumped to +/- 40 K, due, in large part, to the weak fluorescence signal in this region.

Summary/Future Work

2-line temperature and mole fraction imaging of 3-pentanone in an engine cylinder below 600 K has been previously performed with reasonable success [11]. However, as evidenced by the above photophysical experiments and demonstration, fluorescence signal from 248 nm excitation, a commonly used wavelength for this technique, is not strong enough to provide precise information in regions above 600 K,

regions that are quite important to practical combustion applications. We must therefore seek another wavelength within the ketone absorption spectrum where high laser powers are available. The quadrupled output from a YAG laser at 266 nm may afford this opportunity.

Unfortunately, the current literature provides no information on fluorescence signal from 266 nm excitation above 600 K; however, modeling from our acetone work, which we believe will apply quite well to 3-pentanone, indicates that 266 nm excitation will result in higher signals, due to both increased absorption cross-section and a larger fluorescence yield than when excited by 248 nm light. Therefore, we plan to explore the photophysics of 3-pentanone using 266 nm excitation at temperatures up to 900 K. Once this data is obtained, a new temperature mapping up to 900 K, based on 308/266 nm ratioing, should be enabled.

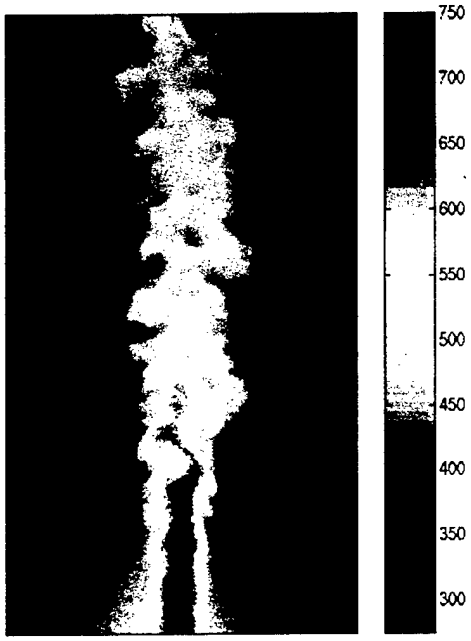

Figure 2.2.7 Single line temperature image of a heated jet using 3% 3-pentanone in nitrogen, excited at 248 nm.

Section 2.2 References

1. Thurber, M., Grisch, F., Kirby, B., Votsmeier, M., and Hanson, R. K., "Measurements and Modeling of Acetone Laser-induced Fluorescence with Implications for Temperature-imaging Diagnostics," *Appl. Optics* **37**, 4963-4978 (1998).

2. Thurber, M, Kirby, B., and Hanson, R. K., "Instantaneous Imaging of Temperature and Mixture Fraction with Dual-Wavelength Acetone PLIF," AIAA-98-0397, *36th AIAA Aerospace Sciences Meeting and Exhibit*, AIAA (1998).

3. Thurber M., Grisch F., Hanson R., "Temperature Imaging with Single- and Dual-wavelength Acetone Planar Laser-Induced Fluorescence," *Optics Lett.* **22**, 251-253 (1997).

4. Thurber, M. C. and Hanson, R. K., "Pressure and Composition Dependence of Acetone Laser Induced Fluorescence with Excitation at 248, 266 and 308 nm," *Appl. Physics B* **69**, 229-240 (1999).

5. Thurber, M. C. and Hanson, R. K., "Simultaneous Imaging of Temperature and Mole Fraction using Acetone Laser-Induced Fluorescence," *Experiments in Fluids*, in press.

6. Wolff, D., V. Beushausen, P Andresen. (1995) "Ketones: Suitable Tracer Substances for Quantitative LIF Measurements in High Pressure Systems," *Thirty-third Japanese Symposium on Combustion.*

7. Grossmann, F., Monkhouse, P. B., Ridder, M., Sick, V. and Wolfrum, J., "Temperature and Pressure Dependences of the Laser-Induced Fluorescence of Gas-Phase Acetone and 3-Pentanone," *Appl. Physics B* **62**, 249-253 (1996).

8. Einecke S., Schulz C., Sick, V., Driezler, A., Schliebl, R. and Ulrich, M., "Two-dimensional Temperature Measurements in an SI Engine Using Two-line Tracer LIF," *SAE Paper* 982468 (1998).

9. Berckmuller, M., Tait, N., Lockett, R., and Greenhalgh, D., "In-cylinder Crank-angle-resolved Imaging of Fuel Concentration in a Firing Spark-ignition Engine Using Planar laser-induced Fluorescence," *25th Symposium (International) on Combustion*, The Combustion Institute (1994).

10. Fujikawa T., Hattori Y., and Aklhama, K., "Quantitative 2-D Fuel Distribution Measurements in an SI Engine Using Laser-Induced Fluorescence with Suitable Combination of Fluorescence Tracer and Excitation Wavelength," *SAE Paper* 972944 (1997).

11. Einecke S., Schulz C., Sick V. "Measurement of Temperature, Fuel Concentration and Equivalence Ratio Fields Using Tracer LIF in IC Engine Combustion," *Appl. Physics B* **71**, 717-723 (2000).

12. Martinez, R., Buitrago, A., Howell, N., Hearn, C., and Joens, J., "The Near U.V. Absorption Spectra of Several Aliphatic Aldehydes and Ketones at 300 K," *Atmospheric Environment* **26A**, 785-792 (1992).

2.3 Development of a TDLAS Probe for Measurements in Hypervelocity Flows

Introduction

Reflected shock tunnels have been providing high-enthalpy flowfields in ground-testing applications for over thirty years [1]. Accurate determination of the steady-state test time in the flowfields is necessary for reliable facility testing and development[2]. To date, researchers have depended on non-equilibrium n-dimensional nozzle codes to calculate the free stream conditions[3-5] with input from facility instrumentation. Operators have relied on experience and traditional radial survey measurements of stagnation pressure and heat-flux gauges to determine flow parameters[6]. Unfortunately, some of the commonly accepted techniques for determining uniform flow conditions (e.g., radiation intensity measurements, Langmuir probes, microwave interferometer measurements) have suggested steady-state test times that were significantly less than those inferred from the Pitot-probe pressure measurements[7]. In addition, stagnation-point heat-flux measurements have been found to be of little value in determining the duration of uniform flow.

An effort was been put forth to develop hypervelocity probes to directly measure temperature, velocity, and concentration in high-speed flows using tunable diode laser absorption spectroscopy (TDLAS) techniques. Through the course of this program robust probes were developed to be installed directly in high-enthalpy flowfields and fiber coupled to rapidly tunable laser sources operating at near-IR wavelengths.

Experimental Measurements

We discuss here measurements using two different TDLAS probes, one for water vapor and one for potassium atoms [8].

Water Measurements

Figure 2.3.1 illustrates schematically the layout of the electronics and optical components within a typical probe and the remote laser control systems. Two H_2O transitions, the $4_{04} \leftarrow 5_{05}$ at 1.40074 nm and the $7_{71} \leftarrow 7_{70}$ at 1.39569 nm, were used. The 1400-nm beam (λ_1) was directed at a 54° angle with respect to the bulk gas velocity. The 1396-nm beam (λ_2) was directed through the test gas 5 times in a multi-pass arrangement to increase the path length.

Figure 2.3.2 presents measured unshifted and Doppler-shifted absorption lineshapes recorded from a single scan at t=3.6 ms in a 10-MJ/kg-enthalpy hypersonic air flowfield seeded with 6% water vapor. The pressure trace (top trace) was recorded using a pitot probe located on the TDL probe to indicate the flowfield development. The test time was defined as the interval in which the pressure remained relatively constant. The predicted flowfield conditions (enthalpy = 10 MJ/kg, bulk gas velocity = 4500 m/s, freestream temperature = 650 K, freestream pressure = 8 torr) were calculated based on

CFD modeling of the facility nozzle and do not include the effects of water in the test gas.

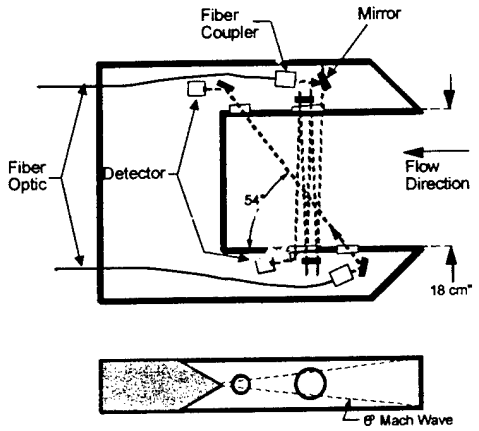

Fig. 2.3.1. A schematic illustrating the laser beam paths and the optoelectronics contained in the two-line water-vapor sensor capable of measuring velocity, temperature, and water vapor partial pressure simultaneously. The side view illustrates the trajectory of the leading edge Mach waves.

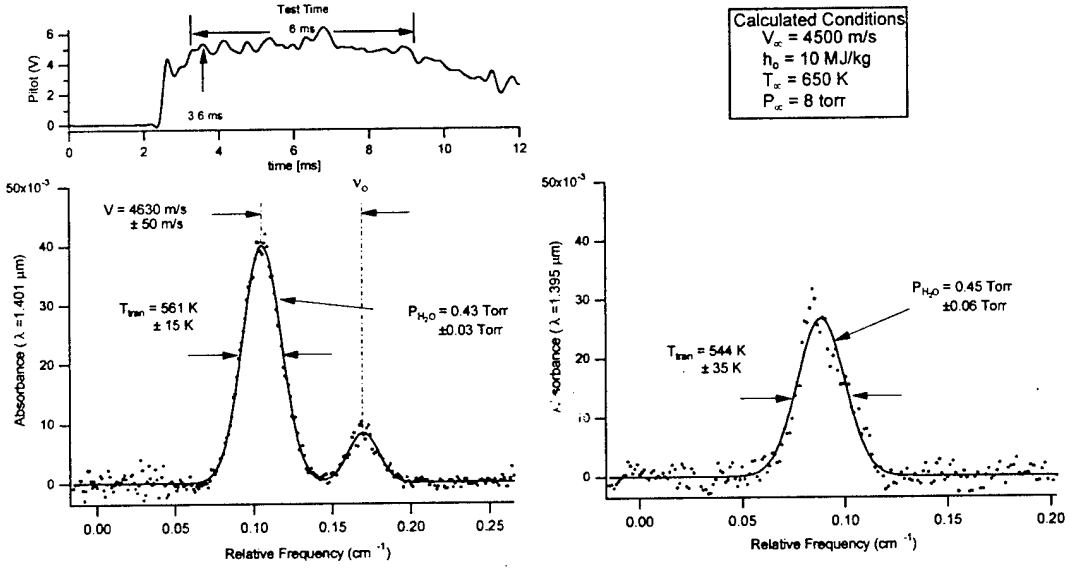

Fig. 2.3.2. (top,left) Pressure trace recorded from a pitot pressure probe during a test run. (bottom left and right) Reduced absorption profiles obtained from a single laser scan (near 1.401 and 1.395 μm respectively) in air seeded with 6% water vapor. The rotation temperature is obtained from the absorbance ratios of the two transitions and is 560 ± 13 K.

Representative absorption traces (recorded at t=3.6 ms) for the probed transitions are shown in the bottom left (λ_1= 1401 nm) and right (λ_2= 1395 nm) of Fig. 2.3.2. Since the total pressure in the flowfields probed was less than 8 torr, collisional broadening was negligible and the measured absorption lineshapes were essentially Gaussian. The smaller amplitude (unshifted λ_1) absorption is due to absorption by (static) gas contained within the probe. The larger amplitude (Doppler-shifted λ_1) absorption is due to relative motion of the test gas in the direction of beam propagation. The relative frequency (Doppler) shift corresponds to a freestream velocity of 4630 m/s. Solid lines represent

the best-fit Gaussian profiles to each data set. Translational temperatures were determined from the width of each (Doppler-broadened) lineshape [T_{trans} = 561 K (λ_1), 544 K (λ_2)] are in excellent agreement with the rotational temperatures determined from the two-line ratio of absorbances (T_{rot} = 560 K).

Figure 2.3.3 presents time histories of the measured total pressure (measured with a facility pitot probe), H_2O partial pressure, gas temperature, and gas velocity in the LENS tunnel for test run using hydrocarbon free air seeded with water vapor (6% by partial pressure). The signal from a pitot probe illustrates the facility timing and is traditionally used to infer the steady test time interval (t = 3 - 9 ms). The three ordinate axes (y-axes) share the same time axis. The first data points plotted correspond to the first laser transmission traces that could be reliably interpreted after the intense flash of broadband emission following facility start up.

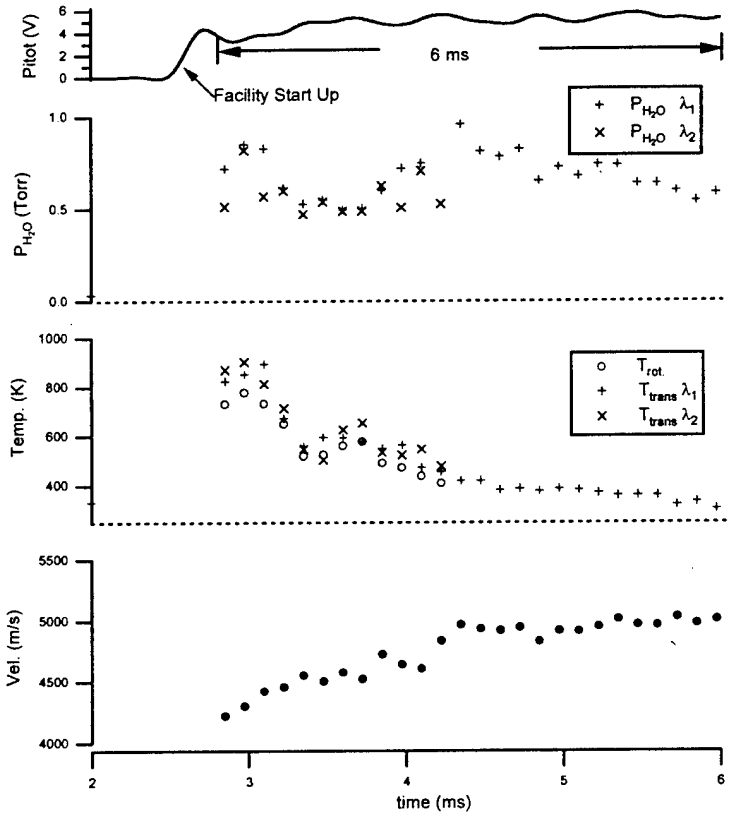

Fig. 2.3.3. Measurements of temperature, velocity and H_2O partial pressure recorded simultaneously in free stream with a flow enthalpy of 10 MJ/Kg in air seeded with 6% H_2O (by pressure). The test time, defined as the interval in which the pitot pressure value was relatively constant, began at t = 3 ms and lasted approximately 6 ms. Measured values of translational and rotational temperature, and velocity are in agreement with CFD-calculated steady-state values (650 K and 4500 m/s, respectively) for a period of approximately 1.0 ms near the test time beginning.

The initial data points reflect the starting process of the nozzle. The initial measured temperatures (t < 3 ms) indicate the presence of hot water (near 900 K) vapor behind the initial shock wave. The fluctuations in the temperature and pressure measurements prior to the test time indicate rapid temporal changes in the flowfield

during the tunnel start up. The measured velocities indicate a relatively gradual increase to a steady value of 4500 m/s, equal to the CFD determined value. The scatter in the temperature measurements are most likely due to the fluctuations (temporal gradients) present in the flow.

The measurements reach relatively constant values between t = 3.2 ms and t = 4.2 ms and are consistent with free-steam conditions (T_∞ = 650 K, V_∞ = 4500 m/s) calculated using CFD models of the nozzle flow which neglected the presence of water in the reflected shock region. During the initial start-up and test-time intervals the rotational and translational temperatures are within 150 K of each other. As the temperature decreases below 420 K, the SNR of the absorption measurement near 1.395 μm (the multiple-pass high-temperature transition) decreases substantially, thus no rotational temperature measurements are reported. Additionally, the velocity increase from 4500 m/s to 5000 m/s near 4.2 ms is accompanied by a temperature decrease. It appears the facility is not operating in a steady fashion. However, assuming that the total enthalpy is steady and the test gas is calorically perfect at the nozzle exit, the associated temperature change would be 2000 K, which is impossible starting from 650 K, and thus indicates enthalpy from chemically frozen species or excited internal states may have been released into the flow or simply added to the reflected shock region.

Potassium-Atom Measurements in the 96-in HST

A probe based on a species other than water was developed based on its absence in test facilities. For example, oxygen-free test gases or the use of helium driver-gas does not generate water. Many potential candidates were reviewed and potassium was selected. Attractive features of a potassium sensor are that it can be smaller due to the large line strengths of the atomic-electronic transitions and the absorption features are narrow relative to those of other atomic absorbers. In the potassium-atom measurement probe described here, the wavelength of the (AlGaAs) diode laser was current tuned at a 10-kHz repetition rate over the potassium D_1 ($^2S_{1/2} \rightarrow {}^2P_{1/2}$) transitions near 770 nm to record a Doppler-shifted absorption feature every 0.1 milliseconds.

Figure 2.3.4 presents representative absorption lineshapes recorded from a single laser scan (0.1 ms) during a tunnel run (9.5-MJ/kg total enthalpy) with air as the test gas. The left panel of Fig. 2.3.8 is a measured spectrum for the probe beam that propagated at an angle to the flow. Three key absorption features can be seen. The smallest amplitude feature (near 0.68 cm^{-1}) is due to absorption by nearly stationary hot gas adjoining the wall in the probe window boundary layer. The larger amplitude feature has been shown (by numerical solutions of the boundary layer equations along with equilibrium chemistry calculations) to include the combined absorption of cold freestream potassium and that of relatively hot potassium atoms in the outer portion of the boundary layer (i.e. the thermal recovery zone). This combined absorption results in an asymmetric overall lineshape for the large absorption feature, with greater width on the right of the peak (labeled "freestream absorption") than on the left. Although the length scales in the boundary layer are small compared to the total absorption pathlength, the concentrations present due to the elevated temperature can be much larger than the freestream. The velocity is

determined from the distinct freestream absorption peak present in each laser sweep, as this narrow peak is associated with the potassium in the fast-moving freestream.

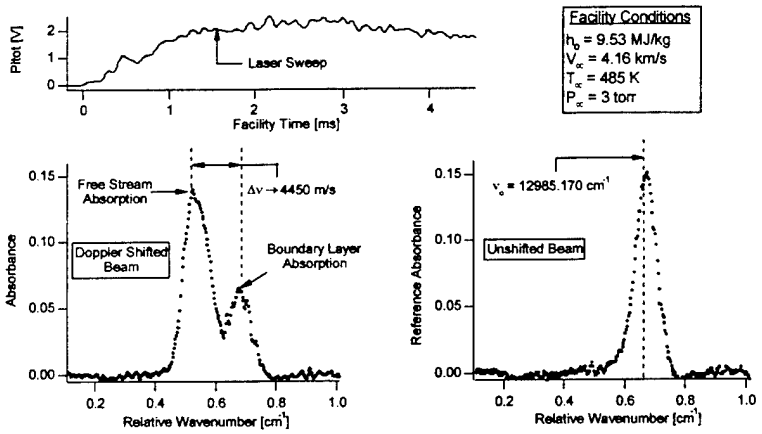

Fig. 2.3.4. (top,left) Pressure trace recorded from a pitot pressure probe during a test run in the Calspan 96" HST. (bottom left and right) Reduced absorption profiles obtained from a single laser scan. The left-hand trace was obtained from a beam directed at a 43.8-deg. angle with respect to the bulk gas flow. The right-hand trace was obtained from a beam directed at a 90.0-deg. angle with respect to the bulk gas flow.

The right panel of Fig. 2.3.4 illustrates a typical absorbance lineshape for the beam propagated orthogonally to the bulk gas velocity. Note that the location of the peak absorbance agrees well with that of the right-hand peak in the left panel of Fig. 2.3.4. The measured Doppler shift for this spectral scan corresponds to a freestream velocity of 4.45 km/s which is in relatively good agreement with the calculated (steady-state) value of 4.16 km/s determined from Calspan computations. The measurement uncertainty in velocity is ±200 m/s, due predominantly to boundary layer absorption.

Figure 2.3.5 presents measurements of the temporal variations of gas velocity during a test with a total enthalpy of 9.53 MJ/kg and a freestream temperature of 485 K. The total pressure measurements were recorded at a 100-kHz rate using a nearby pitot probe. Note that a period of nearly constant pressure and velocity is observed over a period of about 1.9 ms (from t = 1.2 to 3.2 ms in Fig. 2.3.5).

Summary

The development of TDLAS probes for hypersonic flows has enabled more accurate characterization of high-enthalpy impulse facilities. These H_2O-based probes are able to accurately measure H_2O concentration, velocity and temperature in the test stream and have been validated by comparison with potassium-based probes. The capabilities of these probes have been demonstrated in the Calspan facility where the problem of H_2 driver gas contamination was studied.

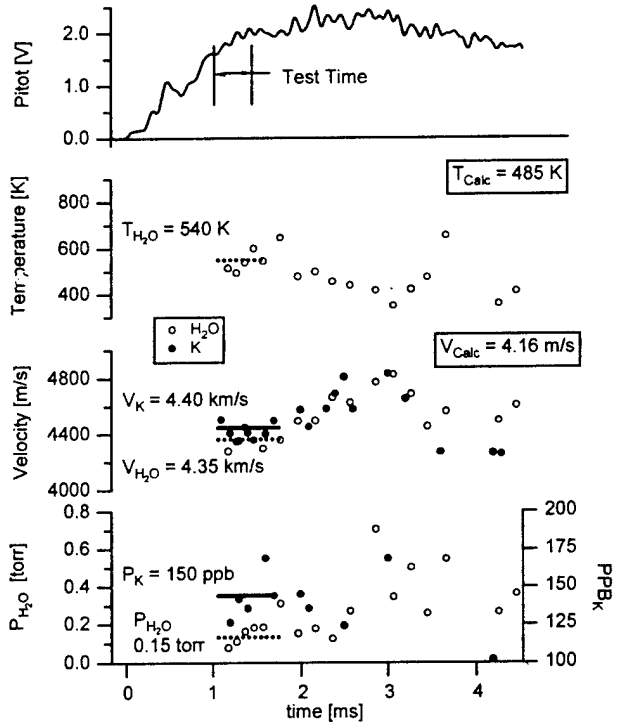

Fig. 2.3.5. Measurements of the facility pitot pressure and velocity (recorded using the potassium-based diode-laser sensor) during a 9.53-MJ/kg test. For comparison, simultaneous results using the water-vapor probe are shown. To aid comparison, lines through the data indicate average values of the measured quantity and the temperature and velocity values calculated by Calspan are shown in boxes to the right.

Section 2.3 References

1. Wittliff, C. E., Wilson, M. R., and Hertzberg, A., "The Tailored-Interface Hypersonic Shock Tunnel," *J. Aerospace Sciences* **26** (1959).

2. Holder, D. W. and Schultz, D. L., "The Duration and Properties of the Flow in a Hypersonic Shock Tunnel," *Progress in Astronautics and Rocketry* **17**, Riddel, F.R. editor, (1962).

3. Lordi, J. A., Mates, R. E., and Moselle, J. R., "Computer Program for the Numerical Solution of Nonequilibrium Expansions of Reacting Gas Mixtures," NASA CR-472 (1979).

4. Chadwick, K. M., et al., "Design and Fabrication of a Mach 8 Contoured Nozzle for the LENS Facility," AIAA 96-0585 (1996).

5. Korte, J. J. and Hodge, J. S., "Prediction and Measurement of Flow Quality in Hypersonic Wind-Tunnel Nozzles Designed Using CFD," AIAA 94-2544 (1994).

6. Park, C., "Evaluation of Real-Gas Phenomena in High-Enthalpy Impulse Test Facilities: A Review," *J. Thermophysics and Heat Transfer* **11**, (1997).

7. Dunn, M. G., "Experimental Study of High-Enthalpy Shock-Tunnel Flow. Part II: Nozzle-Flow Characteristics," *AIAA J.* **7** (1969).

8. S. D. Wehe, D. S. Baer and R. K. Hanson, "Diode-Laser Sensor for Velocity Measurements in Hypervelocity Flows," *AIAA J.* **37**, 1013-1015 (1999).

2.4 High-Pressure H_2O Diagnostics

Measurements of water vapor concentration are directly relevant to combustion, since water vapor concentration can be related to performance parameters such as combustion and propulsion efficiencies, and heat release. In this research program we: 1) developed a comprehensive model of high pressure water spectroscopy, 2) measured critical line-broadening and –shift parameters, 3) performed controlled experiments in a static cell at high number densities to validate line-shape modeling, and 4) validated an H_2O spectral code using shock tube experiments. These measurements were enabled by the development of a diode-laser based H_2O concentration and temperature diagnostic in our laboratory for use in high-pressure and high-temperature environments that took advantage of near-IR H_2O absorption features near 7117, 7185 and 7462 cm^{-1}.

Line-Shape Modeling

A comprehensive line-shape model of neutral molecules was developed. Important spectroscopic phenomena that arise due to independent effects, 1) the breakdown of impact line shapes in the wings, and 2) line mixing due to inelastic collisions, and become important in the modeling of line shapes at high number densities (pressures) have been highlighted. Impact line shapes adequately describe the near-wing region of a true line shape. Effects due to finite duration of collisions, that are neglected by impact line shapes, have to be accounted for in the modeling of the intermediate- and far-wings of an isolated transition at high number densities. At higher number densities, inelastic collisions neglected by the additive approximation result in the blending of transitions leading to the very non-linear effect of line mixing. A decision tree and a road map to choose an appropriate line shape model for the temperature and pressure range of interest were developed.

A spectral code (H_2OTRAN) for calculating H_2O absorption over a range of temperature and pressure was developed. Example spectra at several higher pressures are shown in Fig. 2.4.1. At high pressure, spectral features merge because of collision-broadening, and the use of H_2O absorption as a diagnostic probe required new strategies. Uncertainties in line shape theory, and the temperature dependence of the line-broadening (2γ) and line shift (δ) parameters, lead to requirements for controlled experiments at elevated temperature and pressure.

Line-Broadening Measurements

Spectrally resolved measurements Of H_2O transitions near 7117, 7121 and 7185 cm^{-1}, were performed using diode lasers. Line-shape analyses of the recorded absorption spectra yielded the temperature-dependent self-, N_2-, and CO_2-broadened half-widths. Room-temperature (296 K) half-widths for 8 rovibrational transitions in the $\nu_1+\nu_3$ and $2\nu_1$ vibrational bands were determined from measurements recorded in a multi-pass cell. The temperature dependence of the half-widths for 4 of the transitions were determined from measurements conducted in a heated static cell over a temperature range of 400-1000 K. Room temperature Ar-broadened half-widths of 4 transitions near 7117 cm^{-1}, and temperature exponents for 3 of these transitions over a temperature range of 273-473 K

were also determined [1]. The room-temperature half-widths and temperature exponents were determined to an average accuracy of +8%/-6% and ±9%, respectively, and are in good agreement with theoretical calculations and published half-widths for transitions with the same rotational quantum numbers.

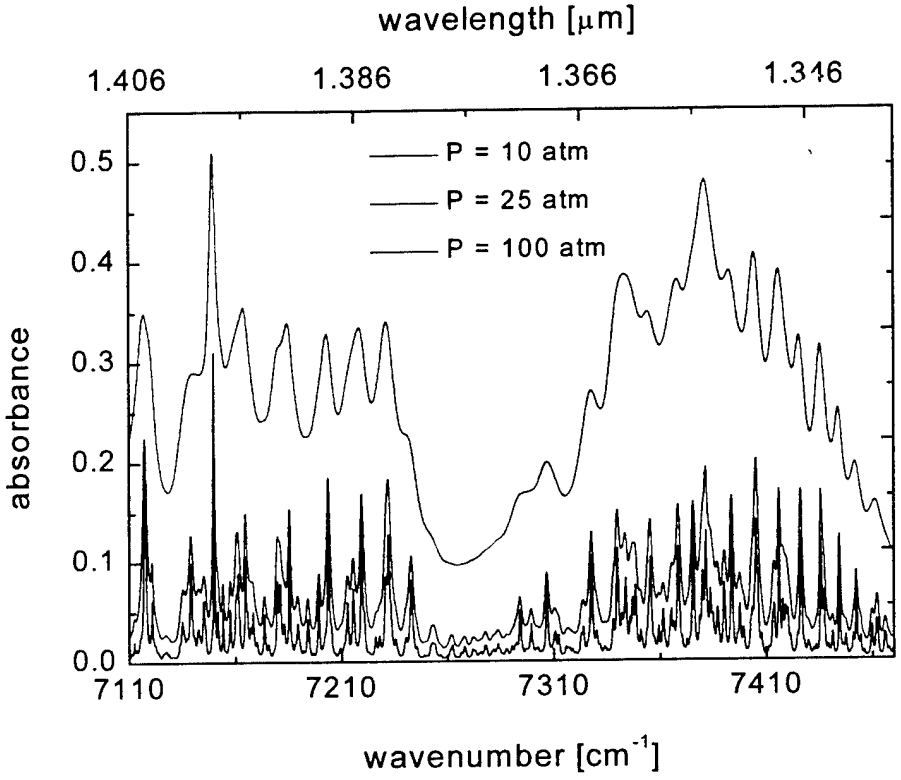

Fig. 2.4.1. High pressure spectroscopy of water-vapor. These spectra were calculated using HITRAN/Delaye at 1000 K, 7% H_2O in N_2 for a pathlength of 5 cm.

Experimental Validation of Line-Shape Modeling

Controlled experiments in a static cell to probe H_2O absorption features at number densities of interest to combustion diagnostics were performed. Good agreement was obtained between recorded data near 7117 cm^{-1} and simulations, based on measured line parameters, leading us to conclude that: 1) effects due to line mixing are negligible for number densities up to 18 amagats, and 2) line shapes based on the impact and the additive approximations could be used in the development of spectroscopic diagnostics to monitor H_2O in high-pressure combustion gases of current interest. Super-Lorentzian behavior, where the recorded data is systematically higher than the simulation, was observed near 7185 cm^{-1}. This was attributed to be due to finite duration of collision effects neglected by the impact line shapes. Due to these observations, the peaks of absorption features were chosen for the development of high-pressure diagnostics.

Shock-Tube Experiments

Water-vapor absorption features near 7117, 7185 and 7462 cm^{-1} were probed at pressures and temperatures to 65 atm and 1800 K, in shock-heated mixtures of H_2O in N_2 and Ar, using diode lasers [2]. Calculated absorbances based on Voigt line shapes and measured line parameters were in good agreement with measured absorbances at 7185.4 and 7117.4 cm^{-1} validating the experimental method and data reduction strategy. As well the present line broadening parameters measurements and measured line positions and strengths due to Toth [3] were found to be in good agreement. Temperature-dependent N_2- and Ar-shift parameters for H_2O absorption features were obtained by shifting the calculated spectra to match the recorded absorption scan. The rapid-scanning method used to these experiments in both static cell and shock tube, permitted the determination of temperature-dependent line-shift parameters over a wide temperature range (293 – 1400 K). Example data are shown in Fig. 2.4.2.

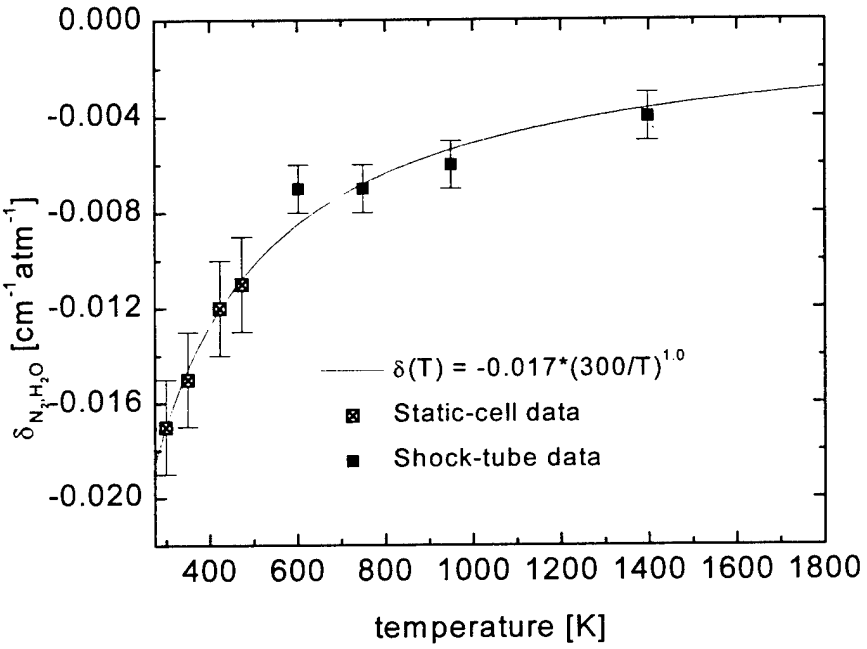

Fig. 2.4.2. Temperature-dependent pressure shifts in water-vapor. Δ_{shift} (cm^{-1}) = δ P(atm).

The measured absorbance at the probed wavelengths were used to ascertain the accuracy of simulation based on current spectroscopic databases. Simulations based on line parameters from HITRAN and HITEMP [4,5] combined with calculated line-broadening parameters from Delaye et al. [6] were found to be similar over the range of temperatures 600-1800 K, and were within 25% of the measurements. The combined use of Toth's (1994) line positions and strengths, and broadening parameters from HITRAN resulted in calculated absorption coefficients that are within 15% of the measurements at all three probed wavelengths.

The model was improved by the use of measured parameters: line-broadening parameters from this study and line positions and strengths from Toth. Improved fits to data are shown in Figs. 2.4.3. H_2OTRAN has been validated for pressures and temperatures up to 60 atm and 1700 K in argon and nitrogen near 7117 and 7185 cm^{-1}.

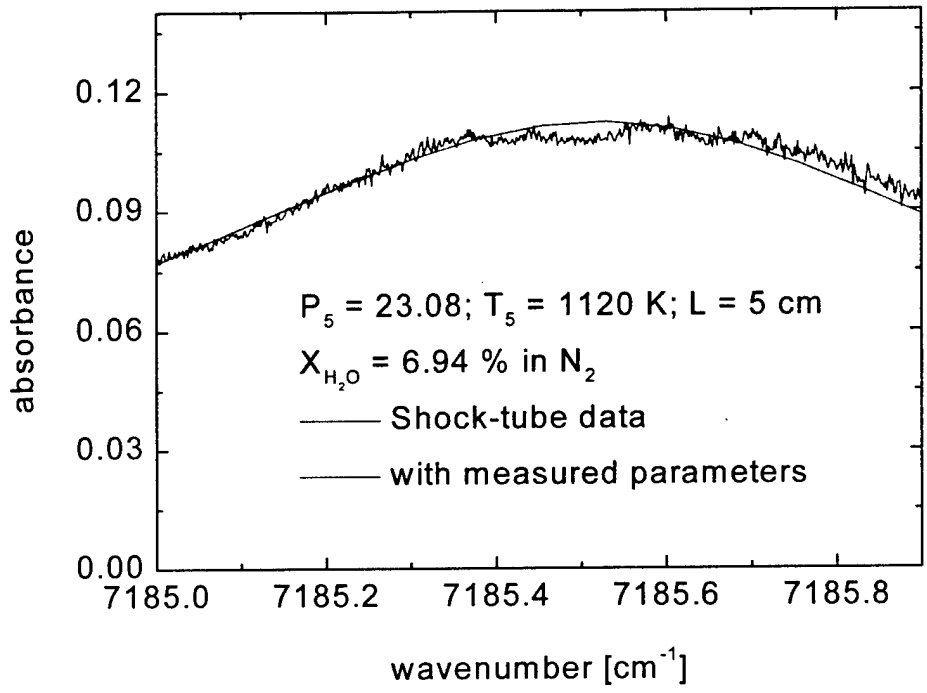

Fig. 2.4.3. Absorption by water-vapor at high pressure: model and data. 23 atm, 1120 K, L =5 cm, 6.94% H_2O in Nitrogen.

Lastly, a design for a diode-laser sensor to monitor water vapor in high-pressure combustion gases was developed [7-9]. The sensor using diode lasers fixed at 7185.4 and 7117.4 cm^{-1} has the potential to simultaneously monitor H_2O mole fraction and temperature, with good sensitivity, in high-pressure and -temperature environments.

Section 2.4 References

1. Nagali, V., Chou, S. I., Baer, D. S. and Hanson, R. K., "Diode-Laser Measurements of Temperature-Dependent Collision Widths of H_2O Transitions in the 1.4 mm Region," *J. Quant. Spectrosc. Radiat. Transfer* **57**, 795-809 (1997).

2. Nagali, V., Herbon, J. T., Horning, D. C., Davidson, D. F. and Hanson, R. K., "Shock Tube Study of High-Pressure H_2O Spectroscopy," *Appl. Optics* **38**, 6942-6950 (1999).

3. Toth, R. A., "Extensive measurements of $H_2{}^{16}O$ frequencies and strengths: 5750 to 7965 cm^{-1}," *Appl. Optics* **33**, 4851-4867 (1996).

4. Rothman, L. S., Gamache, R. R., Tipping, R. H., Rinsland, C. P., Smith, M. A. H., Benner, D. C., Devi, V. M., Flaud, J.-M., Camy-Peyret, C., Perrin, A., Goldman, A., Massie, S. T., Brown, L. R., and Toth, R. A., "The HITRAN molecular database: Editions of 1991 and *1992," J. Quant. Spectrosc. Radiat. Transfer* **48**, 469-507 (1992).

5. Rothman, L. S., Wattson R. B., Gamache R. R., Goorvetech D., Hawkins R. L., Selby J. E. A., Camy-Peyret C., Flaud J.-M., Schroeder J., and McCann A., "HITEMP, the high- temperature molecular spectroscopic database," *J. Quant. Spectrosc. Radiat. Transfer,* in press, (1998) .

6. Delaye, C., Hartmann, J.-M., and Taine, J., "Calculated tabulations of H_2O lines broadening by H_2O, N_2, O_2 and CO_2 at high temperatures," *Appl. Optics* **28**, 5080-5087 (1989).

7. Nagali, V., and Hanson, R. K., "Development of a Diode-Laser Based Diagnostic to Monitor H_2O in High-Pressure Environments," AIAA-97-0774, 35th AIAA Aerospace Sciences Meeting, Reno (1997).

8. Nagali, V., and Hanson, R. K., "Design of a Diode-laser Sensor to Monitor Water Vapor in High-Pressure Combustion Gases," *Appl. Optics* **36**, 9518-9527 (1997).

9. Nagali, V., Herbon, J. T., Horning, D. C., Bates, R. W., Davidson, D. F. and Hanson, R. K., "Diode-Laser Based Diagnostic to Monitor Water-Vapor in High-Pressure Environments," AIAA-99-0942, 37th AIAA Aerospace Sciences Meeting, Reno (1999).

2.5 Diode Laser Sensor for CO Near 2.3 μm

Background

Near-infrared diode lasers provide compact, rugged, and affordable sources of tunable radiation that are compatible with optical fiber components. The wavelength of these laser sources can be tuned to resonance with overtone transitions of small molecules such as CO, CO_2, and H_2O. Thus, diode lasers are attractive as light sources for absorption-based gas sensors that have the potential for measurements of concentrations of specific compounds in reacting gas streams such as the effluent from a combustor. Measurements of multiple transitions from a single molecule enable the measurement of gas temperature as well as effluent species concentration [1,2].

Absorption spectroscopy yields path-averaged concentration and temperature measurements without intrusive probes, which can perturb the gas flow or reaction chemistry. *In-situ* absorption diagnostics avoid the conversion of CO to CO_2, which is a common problem for extractive-sampling probes and can lead to significant under-prediction of the CO concentration by extractive-sampling sensors [3,4]. In addition, *in-situ* measurement can provide real-time monitoring of the effluent, without the inherent time lag for gas transport through an extractive-sampling probe.

The CO measurements reported here are motivated by the need for sensors for emissions monitoring and combustion control applications. Although many of the sensor complications are common to the two applications, there are significant differences in the diagnostic requirements. The time response needed for active combustion control requires measurements directly in the high temperature combustion zone. This significantly increases the complexity of the absorption spectra of the target species and potential interference from other species in the reaction zone. Robust control sensors must have large signal to noise for range of concentrations expected. Sensors for emission monitoring can be located at the effluent exhaust where the gas temperature is much lower and thus the absorption spectra will be less congested. However, these emission measurements are complicated by the entrainment of ambient and/or excess air, which dilutes the target pollutant. In addition, emission compliance sensors must have detection limits well below the regulated emission levels.

The effluent from the combustion of hydrocarbon fuels has large quantities of water vapor. The overtone transitions of CO and CO_2 near 1.55 μm occur near a minima in the H_2O absorption spectra and absorption measurements have been previously reported [5-7]. Unfortunately the weak linestrength of the CO transitions and the large concentration of CO_2 and water vapor in combustion exhaust limits commercial 1.55 μm CO sensors. Recently available tunable diode lasers near 2.3 μm for CO [8] were used in this project to make concentration measurements in the hot combustion gases in a laboratory flame and the moderate temperature effluent in an exhaust duct from the same flame. Gas temperature is determined from the internal energy distribution in water vapor measured by absorption using three different transitions. The CO absorption measurements take advantage of the much stronger linestrengths to improve the detection

limits for both high temperature combustion measurements and moderate temperature combustion effluent measurements.

Experiment

Figure 2.5.1 shows a schematic of the laboratory flame and the diode laser senor arrangement. A premixed ethylene air laboratory flame was stabilized on a 6 cm diameter, water-cooled, flat-flame burner. The fuel-air equivalence ratio was adjusted over the range $0.6 \leq \Phi \leq 1.44$ for a fixed dry-air flow rate of 30.9 slm by adjusting the fuel flow rate between 1.35 and 3.1 slm. The flame was isolated with a nitrogen shroud flow; and the combustor profile was a 6 cm diameter top-hat with less than 8% variation in gas temperature confirmed by thermocouple measurements. The combustor exhaust includes a 1.2 m long, 3.8 cm diameter horizontal exhaust duct with optical access at the ends. The gas temperature decreased linearly along the horizontal duct from 530 to 410K.

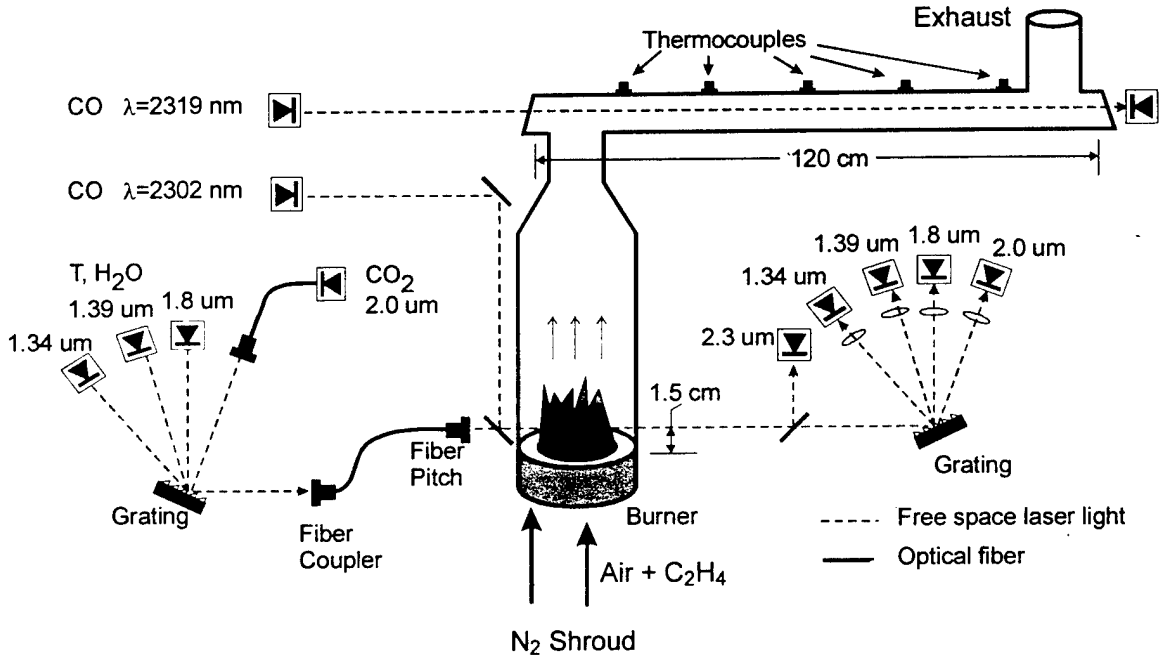

Fig. 2.5.1 Experimental arrangement of diode laser absorption sensors, laboratory flame, and exhaust duct.

Spectral simulation is used to select CO absorption transitions free from interference from water vapor; transitions in the first overtone band R(15) and R(30) were chosen for measurements in the exhaust effluent and combustor respectively [8]. The CO sensors utilized two InGaAsSb/AlGaAsSb ridge-waveguide single mode diode lasers operating near 2.302 μm for R(30) and 2.319 μm for R(15). Absorption measurements in the combustor were made with a 2-pass arrangement, and in the exhaust duct a single pass was used. The transmitted light at these longer wavelengths was detected with an InAs 100 kHz detector.

Light from four individual diode lasers is coupled into a single optical fiber [9] to deliver light to the flame for gas temperature, H_2O, and CO_2 measurements. The

wavelengths of the six diode-lasers were scanned over absorption transitions by individually modulating the injection current with a controlled constant temperature. The H_2O lasers are robust communications grade lasers and were scanned at a 1250 Hz. The CO lasers were prototype lasers and a slower scan rate of 500 Hz was used. Flame emission produced background signals with intensity a few percent of the transmitted laser intensity. This constant flame emission signal was subtracted from the total detected combustion sensor signal before analysis of the optical absorption.

Results

The gas temperature measurements in the combustor vary with fuel/air equivalence ratio between 1700 and 2000 K and are in good agreement with thermocouple measurements. The three water vapor transitions provide a robust gas temperature sensor with a 1 kHz data rate. This is significantly faster than currently available fuel/air control actuators.

Direct absorption measurements of CO recorded in the combustor for a range of fuel/air equivalence ratios produce measured CO concentrations ranging from 300 ppm to 5%. The 0.1-second combustion CO sensor has a signal to noise ratio greater than 10 and a detection limit well below 100 ppm.

Direct absorption measurements of CO concentrations were also made in the exhaust duct using the R(15) transition of the first overtone vibrational band and a sample measurement is shown in Figure 2.5.2. We estimate the noise-equivalent absorbance to be ~3 x 10^{-5} corresponding to 1.5 ppm over the 1.2 m absorption path.

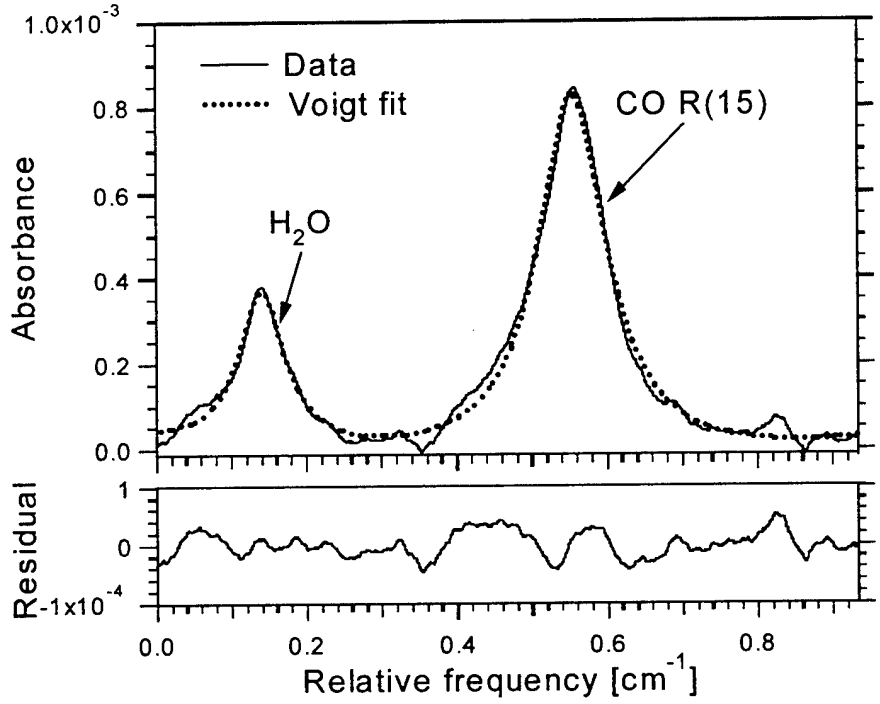

Fig 2.5.2 Interference free direct absorption of 41 ppm of CO in the exhaust duct at 470K.

The CO effluent measured in the exhaust duct depends on fuel/air equivalence ratio. Fuel rich flames have CO concentrations of a few percent; whereas the fuel lean flames have CO effluent less than 20 ppm.

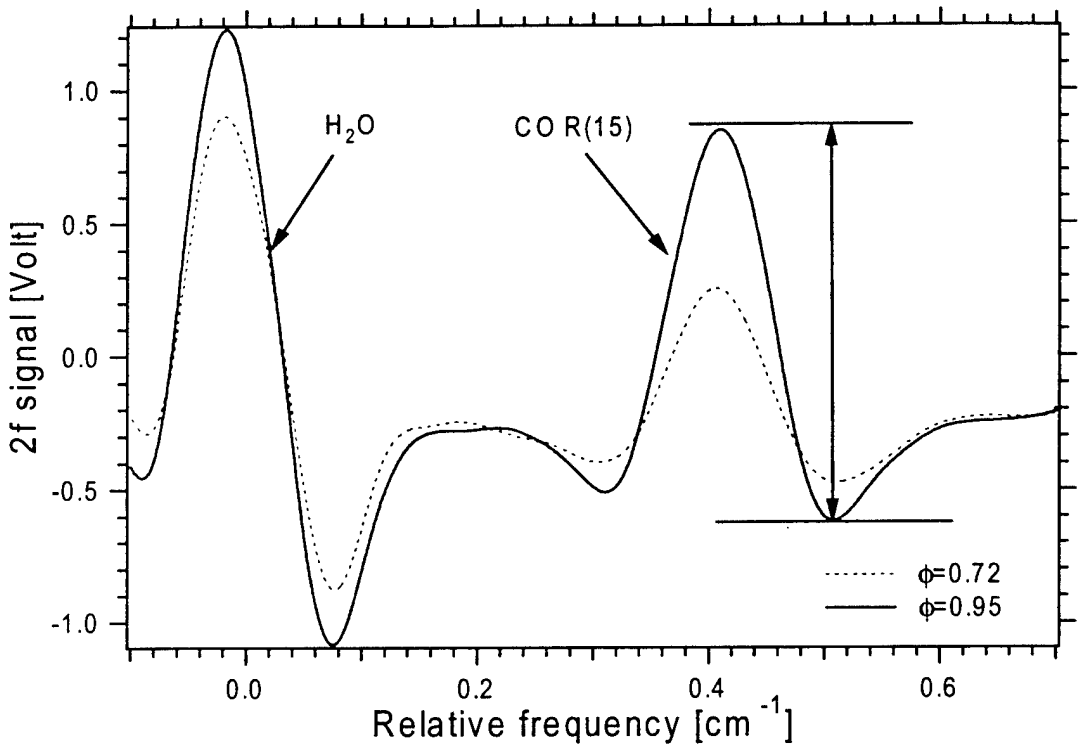

Fig. 2.5.3. Wavelength modulated 2f lineshapes for CO in the exhaust duct; CO concentrations of 6 ppm for $\phi = 0.72$ and 14 ppm for $\phi = 0.95$

Wavelength modulation techniques significantly improve the sensor signal to noise. Figure 2.5.3 shows the lineshapes collected at 2f with a laser modulation at 33 KHz while tuning the mean laser frequency with a 50 Hz ramp for two lean flames Φ=0.72 (CO=6 ppm) and Φ=0.96 (CO=14 ppm). These lineshapes have been averaged over 20 sweeps of the tuning ramp. We estimate using WMS we have a CO detection limit of 0.1 ppm per m path length for a 0.4 second measurement time [8].

Conclusions

We have demonstrated CO, CO_2, H_2O and gas temperature sensors suitable for combustion control application. These sensors are based on optical absorption of diode laser light resonantly tuned to vibrational overtone transitions in the near infrared. These sensors exploit the light sources and fiber optics technologies developed for telecommunications applications.

A CO sensor for combustion effluent was demonstrated with a detection limit of 0.1 ppm for a 1 m path length. Simultaneous detection of CO and CO_2 provides the ratio of CO/CO_2 in the sampled air packet. Measuring the ratio enables determination of amount of mixing of vehicle exhaust with ambient air and thus the total CO emission (in ppm of the total effluent) can be inferred. The temperature variation of the measured

CO/CO_2 ratio is minimized by the judicious choice of monitored transitions; this technique enables a new sensor strategy.

Section 2.5 References

1. Furlong, E.R.; Baer, D.S.; Hanson, R.K.; "Combustion Control and Monitoring using a Multiplexed Diode-Laser Sensor System," Twenty-Seventh Symposium (International) on Combustion, The Combustion Institute, Pittsburgh, 2851-2858 (1996).

2. Webber, M.E.; Kim, S.; Baer, D.S.; Hanson, R.K.; "In situ Combustion Measurements of CO_2 Using Diode Laser Sensors Near 2.0 μm," AIAA Paper 2000-0775, American Institute of Aeronautics and Astronautics, Washington, D.C. (2000).

3. Nguyen, Q.V.; Edgar, B.L.; Dibble, R.W.; "Experimental and Numerical Comparison of Extractive and in situ Laser Measurements of Non-Equilibrium Carbon Monoxide in Lean-Premixed Natural Gas Combustion," *Comb. Flame* **100,** 395-406 (1995).

4. Schoenung, S.M.; Hanson, R.K.; "CO and Temperature Measurements in a Flat Flame by Laser Absorption Spectroscopy and Probe Techniques," *Combust. Sci. Technol.* **24,** 227-237 (1981).

5. Sonnenfroh, D.M.; Allen, M.G.; "Observation of CO and CO_2 Absorption Near 1.57 μm with an External-Cavity Diode Laser," *Appl. Optics* **36,** 3298-3300 (1997).

6. Mihalcea, R.M.; Baer, D.S.; Hanson, R.K.; "Diode Laser Sensor for Measurements of CO, CO_2, and CH_4 in Combustion Flows," *Appl. Optics* **36,** 8745-8752 (1997).

7. Upschulte, B.L.; Sonnenfroh, D.M.; Allen, M.G.; " Measurements of CO, CO_2, OH and H_2O in Room-Temperature and Combustion Gases by Use of a Broadly Current-Tuned Multi-section InGaAsP Diode Laser," *Appl. Optics* **38,** 1506-1512 (1999).

8. Wang, J.; Maiorov, M.; Baer, D.S.; Garbuzov, D.Z.; Connolly, J.C.; Hanson, R.K.; "*In Situ* Combustion Measurements of CO Using Diode-Laser Absorption Near 2.3 μm," *Appl. Optics* **39,** 5579-5589 (2000).

9. Baer, D.S.; Nagali, V.; Furlong, E.R.; Hanson, R.K.; Newfield, M.E.; "Scanned- and Fixed-Wavelength Absorption Diagnostics for Combustion Measurements using Multiplexed Diode Lasers," *AIAA J.* **34,** 489-493 (1996).

2.6 High-Pressure Burner

High-pressure chemically reacting flows are crucial to future Air Force chemical propulsion systems. Initial work has begun to identify the excitation and detection strategy for laser-induced fluorescence imaging of NO molecules in the midst of interference from high-temperature molecular oxygen. We plan to understand the influence of the high-pressure collisional broadening of the NO excitation spectrum and how collisional broadening increases the interference at high temperature where a significant fraction of the oxygen is vibrationally excited. This work requires a high-pressure burner facility where high-temperature/high-pressure LIF experiments can be conducted in a controlled and understandable environment.

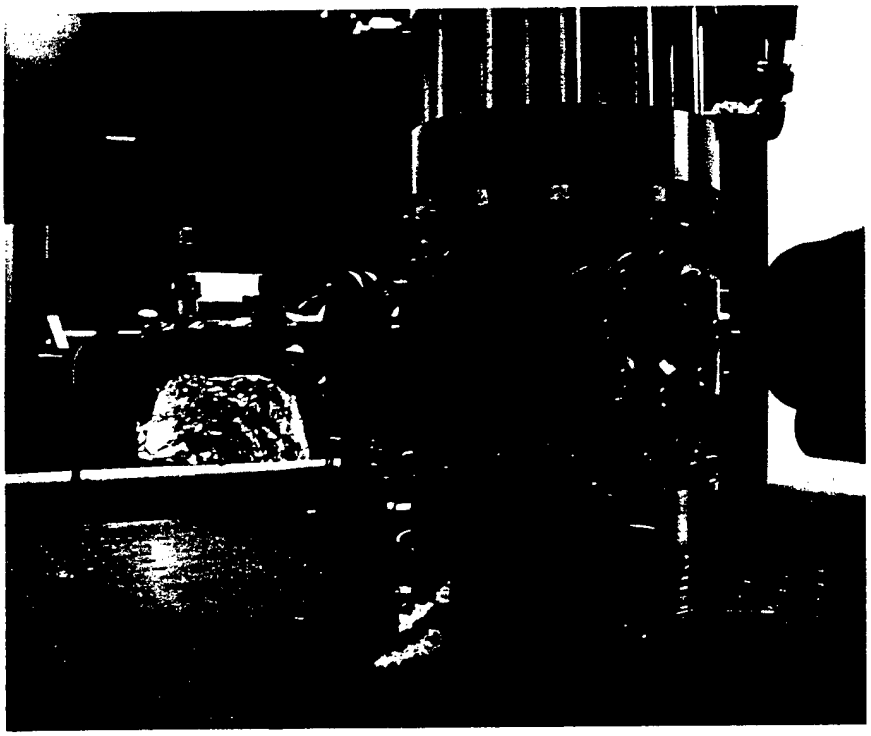

Fig. 2.6.1. Photograph of the High Pressure Burner at Stanford.

During the past contract period we assembled and began initial tests of a high-pressure burner facility. The DLR in Stuttgart agreed to build a version of their 40 bar premixed flat flame burner [1]. This burner, pictured in Fig. 2.6.1, produces a 6 mm diameter premixed flame, stabilized on a porous plug, with flow and pressure control, and is designed for flames at pressures as high as 80 bar. The burner housing has four windows for optical access. Initial flames have been tested at pressures up to 40 bar.

Laser-induced fluorescence (LIF) of NO has become an important tool to understand combustion environments where NO LIF is used to monitor the low-levels formed in the high-temperature combustion environment and to measure important properties such as gas temperature or velocity of flows seeded with trace levels of NO. Previous work in our laboratory [2] identified two difficulties that must be overcome for

routine high pressure LIF at combustion temperatures. The first and most important difficulty is that the spectral features for ultraviolet absorption and subsequent fluorescence of NO and O_2 are overlapped at high temperatures, and this overlap becomes a significant problem when the excitation transitions are collisionally broadened at high-pressure. Thus, the strategies used for NO LIF in atmospheric pressure, fuel lean combustion gases no longer provide PLIF images that distinguish between NO and O_2. Second, we found that the spectroscopic data bases for NO and O_2 at high temperatures and pressures are incomplete and inaccurate; such data are essential to the development and evaluation of measurement strategies which will be successful for the harsh reacting flow environments of interest.

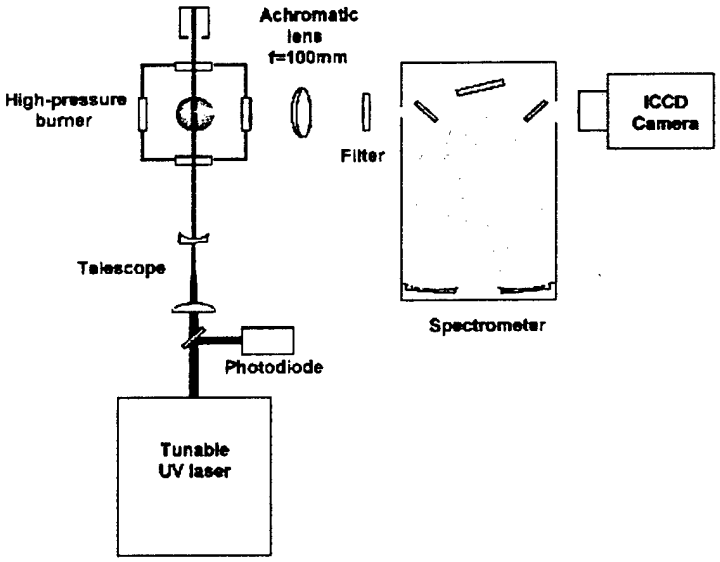

Fig. 2.6.2. Schematic for high pressure LIF experiments.

The arrangement in Fig. 2.6.2 schematically shows the plan for experiments to understand high-temperature/high-pressure NO LIF. Laser-induced fluorescence is excited with light from a frequency doubled dye laser pumped with an Nd:YAG. The fluorescence along the laser beam is imaged onto the slit of a monochromator and the wavelength resolved light is imaged onto a CCD camera.

Thus, at each laser wavelength we collect fluorescence intensity as a function of position in the flame and fluorescence wavelength. We average the fluorescence intensity from the center of the flat-flame and subtract flame luminosity providing a fluorescence wavelength resolved spectrum for each excitation wavelength. Each of these spectra is a horizontal line in the LIF map shown in Fig. 2.6.3. The excitation wavelength is scanned over the region 235.0 and 237.5 nm to excite the 0-1 band of the A-X transition of NO, and the LIF map shown in Fig. 2.6.3 is measured for 1 bar and 40-bar fuel lean (ϕ=0.9) methane/air flames. We observe NO LIF from the few ppm of NO naturally occurring in these flames.

The laser excitation of the 0-1 hot band insures the laser wavelength is optically thin over the wide pressure range. The vertical bars in Fig. 2.6.3 show the Rayleigh and

Mie scattering of this excitation light. As the laser is tuned to excite the NO A-X 0-1, florescence is evident in the 1 bar data from the NO A-X 0-0 band blue (left) of the excitation wavelength. Red of the excitation (right), the signal observed at 1 bar is predominately LIF from other n-1 bands of NO; whereas, in the 40 bar flame significant fluorescence from oxygen is observed.

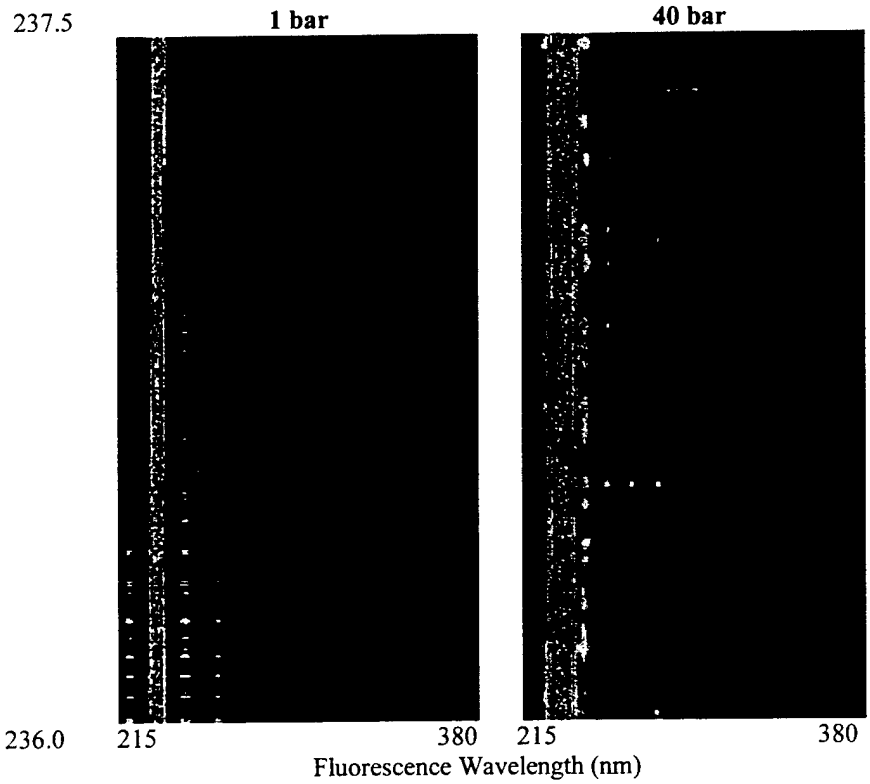

Fig. 2.6.3. Fluorescence wavelength versus excitation wavelength (vertical axis in nm)

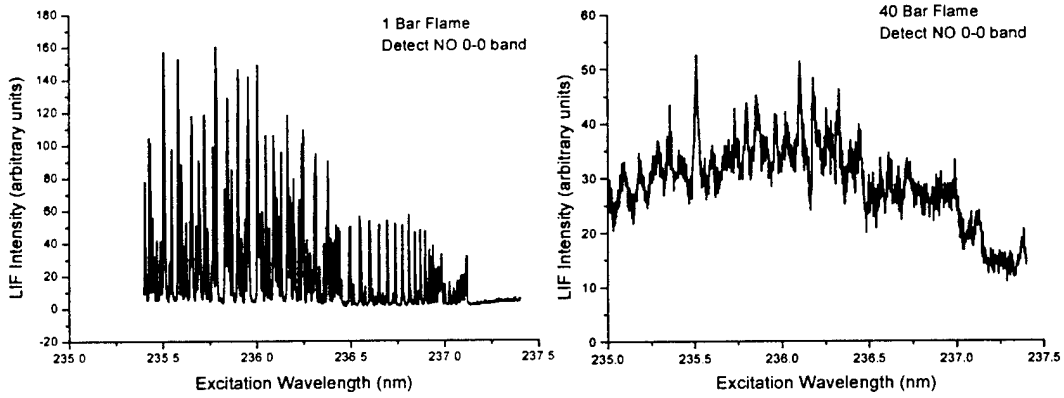

Fig 2.6.4 LIF excitation spectra taken from the data in Fig. 2.6.3 integrating the signal in the NO 0-0 band.

At 40 bar, the features in Fig. 2.6.4 are much broader in laser excitation wavelength reflecting the pressure broadening of the excitation transition. In the 40 bar data the fluorescence signal is contaminated with significant signal from O_2 B-X hot bands. The collisional quenching is now competitive with the predissociation rate and the fluorescence quantum yield for both NO and O_2 vary directly with pressure.

These preliminary experiments illustrate the difficulties choosing the excitation and fluorescence wavelengths to isolate NO LIF at high pressure. Our systematic study of NO LIF strategies will be improved by two modifications to our high-pressure flame facility. First we have modified the gas flow control to seed extra NO into these flames. This will increase the NO signal, allow us to distinguish the high pressure NO LIF, and provide the ability to investigate NO reburn chemistry at high pressure. In addition, we have recently received a new spectrometer and camera. This new equipment will increase the fluorescence spectral resolution by a factor of four. A systematic study of high pressure NO LIF is just beginning.

Section 2.6 References

1. Eberius, H., Just, Th., Kick, Th., Haefner, G., and Lutz, W., "Stabilization of Premixed, Laminar Methane Flames in the Pressure Regime up to 40 Bar," Joint meeting of the German and Italian Sections of the Combustion Institute, 1989.

2. DiRosa, M. D., Klavuhn, K. G., and Hanson, R. K., "LIF Spectroscopy of NO and O_2 in High Pressure Flames" Comb. Sci. Tech. **118**, 257-283 (1996).

3.0 Publications and Presentations

3.1 Refereed Publications

2000

B. J. Kirby and R. K. Hanson, "Design and Analysis of Excitation Schemes for IR PLIF Imaging of CO and CO_2," submitted to *Appl. Optics*, September 2000.

B. J. Kirby and R. K. Hanson, "CO_2 Imaging Using Saturated Planar Laser-Induced Vibrational Fluorescence," submitted to *Appl. Optics*, September 2000.

A. Ben-Yakar and R. K. Hanson, "Ultra-Fast-Framing Schlieren System for Studying the Time Evolution of Jets in Supersonic Crossflows," submitted to *Experiments in Fluids*, October 2000.

A. Ben-Yakar and R. K. Hanson, "Characterization of Expansion Tube Flows for Hypervelocity Combustion Studies in the Flight Mach 8-13 Engine," *J. Prop. and Power*, in press.

B. J. Kirby and R. K. Hanson, "Infrared PLIF Imaging of CO and CO_2," *28th Symp. (International) on Combustion*, Edinburgh, Scotland, July 2000, in press.

J. Wang, S. T. Sanders, J. B. Jeffries and R. K. Hanson, "Oxygen Measurements at High Pressures using Vertical Cavity Surface-Emitting Lasers," *App. Phys. B.*, in press.

B. J. Kirby and R. K. Hanson, "Planar Laser-Induced Fluorescence Imaging of Carbon Monoxide Using Vibrational (Infrared) Transitions," *Appl. Phys. B* **69**, 505-507 (1999).

G. Totschnig, D. S. Baer, J. Wang, F. Winter, H. Hofbauer and R. K. Hanson, "Multiplexed Continuous- Wave Diode-Laser Cavity Ring-Down Measurements of Multiple Species," *Appl. Optics*, **39**, 2009-2016 (2000).

J. Wang, M. Maiorov, J. B. Jeffries, D. Z. Garbuzov, J. C. Connolly and R. K. Hanson, "A Potential Remote Sensor of CO in Vehicle Exhausts using 2.3 μm Diode Lasers," Meas. Sci. Technol. **11**, 1576-1584 (2000).

J. Wang, M. Maiorov, D. S. Baer, D. Z. Garbuzov, J. C. Connolly and R. K. Hanson, "In Situ Measurements of CO using Diode Laser Absorption near 2.3 microns," *Appl. Optics* **39**, 5579-5589 (2000).

1999

E. R. Furlong, R. M. Mihalcea, M. E. Webber, D. S. Baer and R. K. Hanson, "Diode Laser Sensors for Real-Time Control of Pulsed Combustion Systems," *AIAA J.* **37**, 732-737 (1999).

S. D. Wehe, D. S. Baer and R. K. Hanson, "Diode-Laser Sensor for Velocity Measurements in Hypervelocity Flows," *AIAA J.* **37** 1013-1015 (1999).

M. C. Thurber and R. K. Hanson, "Pressure and Composition Dependence of Acetone Laser Induced Fluorescence with Excitation at 248, 266 and 308 nm," *Appl. Physics B* **69**, 229-240 (1999).

V. Nagali, J. T. Herbon, D. C. Horning, D. F. Davidson and R. K. Hanson, "Shock Tube Study of High-Pressure H_2O Spectroscopy," *Appl. Optics* **38**, 6942-6950 (1999).

D. F. Davidson and R. K. Hanson, "Spectroscopic Diagnostics," in Handbook of Shock Waves, Chapter 4.2, G. Ben-Dor, T. Elperin, O. Igra, eds., San Diego, Academic Press (2000).

B. J. Kirby and R. K. Hanson, "Planar Laser-Induced Fluorescence Imaging of Carbon Monoxide using Vibrational (Infrared) Transitions," *Appl. Phys. B* **69**, 505-507 (1999).

R. K. Hanson, D. S. Baer, C. Morris, M. Thurber, E. Furlong and S. Wehe, "Recent Advances in Laser-Based Diagnostics for Gaseous Flows," *J. Visualization* **2**, No. 3/4 (1999).

M. C. Thurber and R. K. Hanson, "Simultaneous Imaging of Temperature and Mole Fraction using Acetone Laser-Induced Fluorescence," *Experiments in Fluids*, in press.

1998

R. M. Mihalcea, D. S. Baer and R. K. Hanson, "Diode-Laser Absorption Sensor System for Combustion Emission Measurements," *J. Meas. Sci. Tech.* **9**, 327-338 (1998).

E. R. Furlong, D. S. Baer and R. K. Hanson, "Real-Time Adaptive Combustion Control Using Diode-Laser Absorption Sensors," 27th Symp. (International) on Combustion, The Combustion Institute, pp. 103-111 (1998).

R. M. Mihalcea, D. S. Baer and R. K. Hanson, "Advanced Diode Laser Absorption Sensor for In-Situ Combustion Measurements of CO_2, H_2O and Temperature," 27th Symp. (International) on Combustion, The Combustion Institute, pp. 95-101 (1998).

R. M. Mihalcea, D. S. Baer and R. K. Hanson, "Diode-Laser Absorption Measurements of CO_2 near 2.0 μm at Elevated Temperatures, *Appl. Optics* **37**, 8341-8347 (1998).

V. Nagali, J. T. Herbon, D. C. Horning, D.F. Davidson and R.K. Hanson, "Shock Tube Study of High-Pressure H_2O Spectroscopy," *Appl. Optics* **38**, 6942-6950 (1999).

T. P. Parr and R. K. Hanson, "Combustion Diagnostics," in *Propulsion Combustion: Fuels to Emissions*, Chap. 9, pp. 281-320 (G.D. Roy, ed.), Taylor and Francis, Washington, DC (1998).

R. M. Mihalcea, D. S. Baer and R. K. Hanson, "Diode-Laser Absorption Sensor System for Combustion Emission Measurements," *J. Meas. Sci. Tech.* **9**, 327-338 (1998).

J. L. Palmer and R. K. Hanson, "Application of the Method of Characteristics to Underexpanded, Free-Jet Flows with Vibrational Nonequilibrium, *AIAA J.* **36**, 193-200 (1998).

M. C. Thurber, F. Grisch, B. J. Kirby, M. Votsmeier and R. K. Hanson, "Measurement and Modeling of Acetone Laser-Induced Fluorescence with Implications for Temperature Imaging Diagnostics," *Appl. Optics* **37**, 4963-4978 (1998).

1997

V. Nagali, S. I. Chou, D. S. Baer and R. K. Hanson, "Diode-Laser Measurements of Temperature-Dependent Collision Widths of H_2O Transitions in the 1.4 μm Region," *J. Quant. Spectrosc. Radiat. Transfer* **57**, 795-809 (1997).

M. C. Thurber, F. Grisch and R. K. Hanson, "Temperature Imaging with Single- and Dual-Wavelength Acetone Planar Laser-Induced Fluorescence," *Opt. Lett.* **22**, 251-253 (1997).

E. L. Petersen, R. W. Bates, D. F. Davidson, and R. K. Hanson, "Development of Laser-Absorption Techniques for Shock Tube Studies at Elevated Pressures," Proc. 21st Int'l. Symp. on Shock Tubes and Waves, July 20-25, 1997, Australia.

R. M. Mihalcea, D. S. Baer and R. K. Hanson, "Diode-Laser Sensor for Measurements of CO, CO_2 and CH_4 in Combustion Flows," *Appl. Optics* **36**, 8745-8752 (1997).

V. Nagali and R. K. Hanson, "Design of a Diode-laser Sensor to Monitor Water Vapor in High-Pressure Combustion Gases," *Appl. Optics* **36**, 9518-9527 (1997).

R. K. Hanson, "Advanced Laser-Based Diagnostics for Shock Tube/Tunnel Flows," plenary paper, Proc. 21st Int'l. Symp. on Shock Tubes and Waves, July 20-25, 1997, Australia.

3.2 Presentations

2000

B. J. Kirby and R. K. Hanson, "Infrared PLIF Imaging of CO and CO_2," 28th Symp. (International) on Combustion, Edinburgh, Scotland, July 2000.

B. J. Kirby and R. K. Hanson, "Dual-Camera Infrared PLIF Imaging of CO and CO2," paper AIAA 2000-0640 at AIAA Aerospace Sciences Meeting, Reno, NV, January 2000.

B. J. Kirby, "Infrared PLIF Imaging Diagnostics for Visualization of CO and CO_2 in Flames," presented at Sandia National Labs Combustion Research Facility, Livermore, CA, September 20, 2000.

B. J. Kirby and R. K. Hanson, "Excitation Schemes for Infrared PLIF Imaging of Carbon Dioxide and Methane," 2000 OSA Annual Meeting, Providence, Rhode Island, October 22-26, 2000.

M. E. Webber, S. Kim, D. S. Baer and R. K. Hanson, "In Situ Combustion Measurements of CO2 using Diode Laser Sensors Near 2.0 um," paper AIAA 2000-0775 at AIAA Aerospace Sciences Meeting, Reno, NV, January 2000.

J. Wang and R. K. Hanson, "In Situ CO Exhaust Measurements Using Diode Laser Absorption near 2.3 Microns," 2000 OSA Annual Meeting, Providence, Rhode Island, October 22-26, 2000.

1999

D. S. Baer, S. Sanders, S. Wehe and R. K. Hanson, "Diode-Laser Absorption sensors for Realtime in situ Measurements," invited presentation at OSA Annual Meeting, Santa Clara, CA, October 1999.

S. D. Wehe, D. S. Baer and R. K. Hanson, "Measurements of Gas Temperature and Velocity in High Enthalpy Flows using a Diode Laser Absorption Sensor," 1998 OSA Annual Meeting, October, 1998, Baltimore, MD.

T. Rossmann, M. G. Mungal and R. K. Hanson, "A New Facility for High Compressibility Mixing Layer Studies," AIAA-99-0415 Aerospace Sciences Meeting, January, 1999, Reno, NV.

V. Nagali, J. Herbon, D. Horning, R. Bates, D. Davidson and R. Hanson, "Diode-Laser Based Diagnostic to Monitor Water-Vapor in High-Pressure Environments," AIAA-99-0942 at Aerospace Sciences Meeting, January, 1999, Reno, NV.

A. Ben-Yakar and R.K. Hanson, "Stability and Self-Ignition of Cross-flow Jets and the Influence of Cavity Flame-holders in Supersonic Combustion," AIAA-99-0484 at Aerospace Sciences Meeting, January, 1999, Reno, NV.

R.K. Hanson, D.S. Baer, C. Morris, M. Thurber, E. Furlong and S. Wehe, "Recent Advances in Laser-Based Diagnostics for Gaseous Flows," invited plenary paper, SPIE/VSJ, Yokohama, December 7-9, 1998; also J. Visualization **2**, No. 3/4 (1999).

B.J. Kirby and R.K. Hanson, "Infrared PLIF Imaging of CO and CO_2," paper AIAA-99-0775 at 37th AIAA Aerospace Sciences Meeting, January, 1999, Reno, NV.

S.D. Wehe, D.S. Baer, R.K. Hanson and K.M. Chadwick, "Gas Temperature and Velocity Measurements in Hypervelocity Flows Using Diode-Laser Absorption Sensors," 22nd Int'l. Shock Tube and Shock Wave Symp., London, UK, June, 1999.

1998

R.M. Mihalcea, M.E. Webber, D.S. Baer and R.K. Hanson, "Diode Laser Sensor for Combustion Emissions Monitoring," SPIE/VSJ, Yokohama, December 7-9, 1998.

M. C. Thurber, B. J. Kirby and R. K. Hanson, "Instantaneous Imaging of Temperature and Mixture Fraction with Dual-Wavelength Acetone PLIF," paper AIAA-98-0397 36th AIAA Aerospace Sciences Meeting, Reno, NV, Jan. 12-15, 1998.

A. Ben-Yakar, M. Kamel, C. I. Morris and R K. Hanson, "Hypersonic Combustion and Mixing Studies Using Simultaneous OH-PLIF and Schlieren Imaging," paper AIAA-98-0940 at 36th AIAA Aerospace Sciences Meeting, Reno, NV, Jan. 12-15, 1998.

R. M. Mihalcea, D. S. Baer and R. K. Hanson, "Advance Diode Laser Absorption Sensor for In-Situ Combustion Measurements of CO_2, H_20 and Gas Temperature," AIAA 98-0237 36th AIAA Aerospace Sciences Meeting, Reno, NV, Jan. 12-15, 1998.

B. J. Kirby and R. K. Hanson, "Infrared PLIF Imaging of Gaseous Flows, AIAA-98-0307 36th AIAA Aerospace Sciences Meeting, Reno, NV, Jan. 12-15, 1998.

R. K. Hanson, "Advanced Laser-Based Diagnostics for Shock Tube/Tunnel Flows," plenary paper, Proc. of the 21st Int'l. Symp. on Shock Tubes and Waves, held July 20-25, 1997, Australia.

A. Ben-Yakar, M. Kamel, C. Morris and R. K. Hanson, "Cavity Flame-Holders for Ignition and Flame Stabilization in Scramjets: A Review and an Experimental Study,"

AIAA-98-3122, 34th AIAA Joint Propulsion Conference, July 13-15, 1998, Cleveland, OH.

R. M. Mihalcea, D. S. Baer and R. K. Hanson, "Combustion Emissions Measurements using Diode-Laser Absorption Sensors, AIAA-98-3948, 34th AIAA Joint Propulsion Conference, July 13-15, 1998, Cleveland, OH.

E. R. Furlong, D. S. Baer and R. K. Hanson, "Diode-Laser Sensors for Real-Time Control of Temperature and H_2O in Pulsed Combustion Systems," AIAA-98-3949, 34th AIAA/ASME/SAE/ASEE Joint Propulsion Conference, July 13-15, 1998, Cleveland, OH.

G. S. Feller, I-F. Wu, T. Day, R. J. Menna, R. U. Martinelli, J.C. Connolly, R.M. Mihalcea, D.S. Baer and R.K. Hanson, "Continuously Tunable, Single Mode, External Cavity Diode Lasers at 2 μm," OSA LACEA (Laser App. to Chem. Envir. Analysis) Meeting, March, 1998, Orlando, FL.

R. M. Mihalcea, D. S. Baer and R. K. Hanson, "Diode-Laser Sensing System for Combustion Monitoring," OSA LACEA (Laser App. to Chem. Envir. Analysis), March, 1998, Orlando, FL.

R. M. Mihalcea, D. S. Baer, R. K. Hanson and G. S. Feller, "Diode-Laser Absorption Measurements of CO_2, H_20 and N_20 near 2 μm," OSA LACEA (Laser App. to Chem. Envir. Analysis), March, 1998, Orlando, FL.

E. R. Furlong, D. S. Baer and R. K. Hanson, "Real-Time Adaptive Combustion Control Using Diode-Laser Absorption Sensors," WSS/CI paper 98S-9, March, 1998, Berkeley, CA.

M. E. Webber, R. M. Mihalcea, D. S. Baer, R. K. Hanson, J. Segall and P. DeBarber, "Diode Laser Absorption Measurements of Hydrazine and Monomethylhydrazine," AIAA-98-0400, 36th Aerospace Sciences Meeting, Jan. 12-15, 1998, Reno, NV.

R. M. Mihalcea, D. S. Baer and R. K. Hanson, "Advanced Diode Laser Absorption Sensor for In-Situ Combustion Measurements of CO_2, H_2O and Temperature," WSS/CI paper 98S-21, March 23-24, 1998, Berkeley, CA.

Ben-Yakar, M. Kamel, C. Morris and R. K. Hanson, "Experimental Investigation of Hydrogen-Air Autoignition and Flame Stabilization in Hypervelocity Flows," WSS/CI paper 98S-40, March 23-24, 1998, Berkeley, CA.

1997

E. L. Petersen, R. W. Bates, D. F. Davidson, and R. K. Hanson, "Development of Laser-Absorption Techniques for Shock Tube Studies at Elevated Pressures," Proc. of the 21st Int'l. Symp. on Shock Tubes and Waves, held July 20-25, 1997, Australia.

4.0 Personnel

Individual researchers partially or fully supported by the program during the reporting period are listed below. All the work has been carried out in the High Temperature Gasdynamics Laboratory, in the Department of Mechanical Engineering, under the supervision of Professor R. K. Hanson.

Postdoctoral Research Associates

Doug Baer, Tom Jenkins, Jay Jeffries

Graduate Research Associates

Adela Ben-Yakar
Andrew Chang
Jeff Colwell
Ted Furlong
Brian Kirby
Jon Koch
Radu Mihalcea
Venu Nagali
Mark Thurber
Jian Wang
Shawn Wehe

Ph.D Degrees Awards (1997-2000)

Adela Ben-Yakar, "Experimental Investigation of Mixing and Ignition of Transverse Jets in Supersonic Crossflows"

Edward Furlong, "Diode-Laser Absorption Spectroscopy Applied for the Active Control of Combustion"

Radu Mihalcea, "CO and CO_2 Measurements in Combustion Environments Using External Cavity Diode Lasers"

Venu Nagali, "Diode Laser Study of High-Pressure Water-Vapor Spectroscopy"

Mark Thurber, "Acetone Laser-Induced Fluorescence for Temperature and Multiparameter Imaging in Gaseous Flows"

Shawn Wehe, "Development of a Tunable Diode Laser Probe for Measurements in Hypervelocity Flows"

5.0 Significant Interactions

In addition to the interactions associated with the presentations and publications listed in Section 3 we have had numerous visitors to our laboratory during the contract period. Foreign visitors have come from Germany, China, Australia, and Japan; industrial and national laboratory visitors have included representatives from:

Aerometrics
Boeing
Horiba Instruments
IHI Ltd
Metrolaser
Physical Sciences, Inc.
TRW
United Technologies

Army Research Laboratories (ARL)
NASA Ames
NASA Lewis
Sandia Albuquerque
Sandia Livermore.

Also during this period, Professor Hanson has given invited presentations on AFOSR-sponsored diagnostics research to several industrial laboratories, universities, and government groups. Members of our group have provided technical information and advice, by telephone and mail, to several external researchers interested in duplicating or extending our diagnostics concepts.

6.0 Inventions

A provisional patent application has been filed by Jian Wang and Ronald K. Hanson for an invention called "Temperature-Independent Measurements of Gas Concentration". This invention was supported in part by grant number F49620-98-1-0010 awarded by the Air Force Office of Scientific Research.

This invention relates generally to using spectroscopic techniques for gas concentration measurements, and in particular to using a ratio of gas concentrations to obtain temperature-independent measurements. This method is especially valuable for gas sensing applications where the temperature of probed gas medium is non-uniform and unknown, such as remote sensing of exhaust from vehicles.

7.0 Technology Transitions/Transfers

PLIF Imaging in Rocket Exhaust
Performer: R. K. Hanson, Stanford Unversity
Customer: Dr. Larry Cohen, Aerojet Corporation, Sacramento, CA
Result: Species concentration imaging in liquid rocket engines
Application: Data confirming suspected oxidizer nonuniformity in Titan IV stage 1 engine

IR Imaging for Joint Strike Fighter
Performer: R. K. Hanson, Stanford University
Customer: Kondala Saripalli, Boeing Corp., St Louis, MO
Result: CO_2 imaging strategies
Application: Hot gas ingestion monitoring during landing of STOVL Joint Strike Fighter

Water Vapor and Oxygen Measurements
Performer: R. K. Hanson, Stanford University
Customer: Dr. Mark Allen, Physical Sciences, Inc., Andover, MA
Result: Muliplexed laser measurements of O_2, H_2O and temperature
Application: Development of commercial diode laser sensors for industrial furnaces

Spectroscopic Data for Ammonia
Performer: R.K. Hanson, Stanford University
Customer: Peter deBarber, Metrolaser, Irvine, CA
Result: Multiplexed laser absorption measurements of species and temperature
Application: Diode laser and Fiberoptic sensors for industrial process measurement and control

PLIF Imaging in SCRAMJETS
Performer: R. K. Hanson, Stanford University
Customer: Dr. Campbell Carter, Innovative Sci. Sol., Inc., Dayton, OH
Result: Physics of planar-laser-induced fluorescence of species and temperature
Application: Work at WPAFB: OH PLIF in hydrocarbon SCRAMJET flowfield to determine location/extent of burning region

PLIF Imaging in Flames
Performer: R. K. Hanson, Stanford University
Customer: Dr. Campbell Carter, Innovative Sci. Sol., Inc., Dayton, OH
Result: Physics of planar-laser-induced fluorescence of species and temperature
Application: Work at WPAFB: OH/CH PLIF in nonpremixed flames for CFD code validation

Hypersonic Velocity
Performer: R.K. Hanson, Stanford University
Customer: Dr. Ken Chadwick, Calspan Corp., Buffalo, NY
Result: Single-wavelength diode laser velocity sensor using potassium vapor absorption
Application: Instrumentation for hypersonic shock tunnel aerodynamics and propulsion research and development

Spectroscopic Data for Water Vapor
Performer: R.K. Hanson, Stanford University
Customer: Dr. Mark Allen, Physical Sciences, Inc., Andover, MA
Result: Near-infrared absorption data for water vapor
Application: Diode laser sensing in aeropropulsion systems

Shock Tunnel Flow Properties and Test Time
Performer: R.K. Hanson, Stanford University
Customer: Dr. Ken Chadwick, Calspan Corp., Buffalo, New York
Result: Dual-wavelength diode laser sensor for gasdynamic properties and water vapor
Application: Instrumentation for hypersonic shock tunnel aerodynamics and propulsion research and development

Rapid Temperature Sensing and Combustor Control
Performer: R.K. Hanson, Stanford University
Customer: Dr. Klaus Schadow, Naval Air Warfare Center Weapons Division, China Lake
Result: Multiplexed diode-laser sensor for temperature and water vapor
Application: Rapid-response sensor and control algorithms for combustion control

Rapid-response Emissions Monitor
Performer: R.K. Hanson, Stanford University
Customer: Dr. Klaus Schadow, Naval Air Warfare Center Weapons Division, China Lake
Result: Diode-laser sensing in a multipass cell using a fast-sampling probe and 1.5-2.0 micron lasers
Application: Sensitive measurements of CO and unburned hydrocarbons in the exhaust of a 50-kW forced combustion incinerator